The VINE complex is a VPS9-domain GEF-containing SNX-BAR coat involved in endosomal sorting

Author List:

Shawn P. Shortill[1,2], Mia S. Frier[1,2], Michael Davey[2], Elizabeth Conibear[1,2,¥]

1. Department of Medical Genetics, University of British Columbia, Vancouver, BC VH6 3N1, Canada
2. Centre for Molecular Medicine and Therapeutics, British Columbia Children's Hospital Research Institute, University of British Columbia, Vancouver, BC V5Z 4H4, Canada

[¥] Correspondence: Elizabeth Conibear, conibear@cmmt.ubc.ca

Running title: VINE is an endosomal GEF and SNX-BAR coat complex

Keywords: Vrl1, Endosome, Sorting, SNX-BAR, Ykr078w, Vps5, Retromer, VINE, VARP, GEF

Abstract

Membrane trafficking pathways perform important roles in establishing and maintaining the endolysosomal network. Retrograde protein sorting from the endosome is promoted by conserved SNX-BAR-containing coat complexes including retromer which enrich cargo at tubular microdomains and generate transport carriers. In metazoans, retromer cooperates with VARP, a conserved VPS9-domain GEF, to direct an endosomal recycling pathway. The function of the yeast VARP homolog Vrl1 has been overlooked due an inactivating mutation in commonly studied strains. Here, we demonstrate that Vrl1 has features of a SNX-BAR coat protein and forms an obligate complex with Vin1, the paralog of the retromer SNX-BAR protein Vps5. Unique features in the Vin1 N-terminus allow Vrl1 to distinguish it from Vps5, thereby forming what we have named the VINE complex. VINE occupies endosomal tubules and promotes the delivery of a conserved mannose 6-phosphate receptor-like protein to the vacuolar membrane. In addition to sorting functions, membrane recruitment by Vin1 is essential for Vrl1 GEF activity, suggesting that VINE is a multifunctional coat complex that regulates trafficking and signaling events at the endosome.

Introduction

Transport of proteins and lipids at the endosome requires the concerted action of peripheral cargo-sorting complexes, Rab-family GTPases, membrane tethering complexes and soluble *N*-ethylmaleimide-sensitive factor attachment protein receptor (SNARE) proteins (Barr and Lambright, 2010; Burd and Cullen, 2014; Jahn and Scheller, 2006; Numrich and Ungermann, 2014; Pfeffer, 2017; Stenmark, 2009; van Weering et al., 2010). Guanine nucleotide exchange factors (GEFs) belonging to the conserved VPS9 family are important regulators of endosomal function that activate endosomal Rab5-like GTPases (Carney et al., 2006; Delprato and Lambright, 2007). In yeast, the VPS9-domain GEFs Muk1 and Vps9 stimulate the endosomal Rabs Vps21, Ypt52 and Ypt53 to perform downstream functions including activating phosphoinositide 3-kinase (PI3K) to produce the anionic lipid species phosphatidylinositol 3-phosphate (PI3P; Christoforidis et al., 1999; Hama et al., 1999; Paulsel et al., 2013; Peplowska et al., 2007; Singer-Krüger et al., 1994). Together, PI3P and endosomal Rabs are important determinants of endosomal identity and are responsible for recruiting effectors, including coat proteins and vesicle tethers, to the endosomal membrane.

Sorting nexins (SNXs) are a conserved family of proteins that perform direct roles in endosomal trafficking by binding to transmembrane cargo proteins and enriching them into sorting domains (Carlton et al., 2005; Hong, 2019). SNXs localize to the endosome through conserved Phox homology (PX) domains that typically recognize PI3P (Cheever et al., 2001; Xu et al., 2001). A sub-family of SNXs known as SNX-BARs additionally contain a Bin/Amphiphysin/RVS (BAR) domain that mediates dimerization with other

66 BAR domain-containing proteins and imparts membrane binding/deforming properties (Frost et al., 2009;
67 van Weering et al., 2012, 2010). These SNX-BAR dimers, which are capable of deforming cargo-rich
68 membranes into sorting tubules, are emerging as important regulators of protein transport. The seven SNX-
69 BAR proteins present in yeast include the conserved retromer subunits Vps5 and Vps17 (Horazdovsky et
70 al., 1997), the SNX8 homolog Mvp1 (Suzuki et al., 2021), the SNX4 homolog Snx4 and its partners Snx41
71 and Atg20 (SNX7 and SNX30 in humans, respectively; Hettema et al., 2003) and the Vps5 paralog
72 Ykr078w. Retromer and Snx4 complexes promote cargo sorting from the endosome and vacuole (Arlt et
73 al., 2015; Suzuki and Emr, 2018), while Mvp1 appears to function only at the endosome (Suzuki et al.,
74 2021). There is no known function for Ykr078w, which lacks a clear subcellular localization.

75 The best characterized of these SNX-BAR-containing complexes is the heteropentameric retromer
76 complex, which is composed of the Vps26-Vps35-Vps29 trimer and the Vps5-Vps17 SNX-BAR dimer
77 (Seaman et al., 1998). Retromer localizes to PI3P-rich membranes where it promotes the retrograde sorting
78 of cargo including the well-characterized carboxypeptidase Y (CPY) receptor Vps10 (Bean et al., 2015;
79 Burda et al., 2002; Seaman et al., 1998, 1997). In metazoans, the term retromer refers specifically to the
80 VPS26-VPS35-VPS29 trimer which associates with a variety of adaptor proteins including SNXs to
81 promote cargo sorting (Cullen and Korswagen, 2012; Gallon and Cullen, 2015). Mutations in VPS35 have
82 been linked to neurodegenerative conditions including Parkinson's disease and Alzheimer's disease
83 (Mohan and Mellick, 2017; Rahman and Morrison, 2019; Vilariño-Güell et al., 2011; Wen et al., 2011;
84 Zimprich et al., 2011), establishing a connection between endosomal transport machinery and human
85 neurological health.

86 We previously identified a physical association between yeast retromer and the VPS9-domain GEFs Vps9
87 and Muk1, whose activity is required to maintain endosomal pools of PI3P for retromer recruitment (Bean
88 et al., 2015). We also identified a novel VPS9-domain protein, Vrl1, which is mutated and non-functional
89 in strains previously used for trafficking studies. Vrl1 can function as the sole VPS9-domain GEF to
90 stimulate production of endosomal PI3P. Notably, the metazoan homolog of Vrl1, VARP, physically
91 associates with retromer to drive an endosome to plasma membrane sorting pathway (Hesketh et al., 2014).
92 Here, we show that Vrl1 is a member of the SNX-BAR protein family and that it specifically binds the
93 Vps5 paralog Ykr078w/Vin1 to form what we now call the VINE complex. Our results suggest that VINE
94 is both a VPS9-domain GEF and a distinct endosomal sorting complex that operates alongside the retromer,
95 Mvp1 and Snx4 pathways.

96

Results

Vrl1 is a predicted PX-BAR protein that interacts with conserved machinery at the endosome.

In addition to a conserved VPS9 GEF domain, Vrl1 and VARP share a conserved N-terminus and an ankyrin repeat domain (AnkRD) that are not found in other yeast VPS9-domain GEFs (Figure 1A). Vrl1 also features an unannotated region of ~350 amino acids (aa) downstream of the ankyrin repeats that is not present in VARP. The protein fold recognition program Phyre2 (Kelley et al., 2015) identified a PX-BAR module with very high confidence (98.6%) in this region (aa 737-1089; Figure 1 S1A), and ab initio modeling of this region by the AlphaFold2-powered ColabFold program (Mirdita et al., 2021) predicted a structure with striking similarity to the PX-BAR fold (Figure 1B). Because the predicted Vrl1 PX domain is missing key residues for PI3P binding (Figure 1 S1B), we refer to it as a "PX-like" domain. To our knowledge, Vrl1 is the first VPS9 domain-containing protein with predicted structural homology to the SNX-BAR family.

We found that Vrl1, when C-terminally tagged with the bright GFP variant Envy, was present at perivacuolar puncta that colocalize with the endosomal marker Did2-mRuby2, but not the Golgi protein Sec7-dsRed (56% and 2%, respectively, $P < 0.0001$; Figure 1C and 1D). These observations indicate that unlike other yeast VPS9-domain GEFs (Paulsel et al., 2013), Vrl1 constitutively localizes to endosomes. To identify endosomal partners of Vrl1, we performed a protein fragment complementation assay (PCA) based on a drug-resistant variant of the dihydrofolate reductase (DHFR) enzyme (Figure 1E; Michnick et al., 2010; Tarassov et al., 2008). Proximity between two proteins that are fused to complementary DHFR fragments reconstitutes enzyme activity and confers resistance to the inhibitor methotrexate. Full length Vrl1, and a cytosolic fragment of Vrl1 lacking the AnkRD, PX-like and BAR domains (Figure 1 S2A), were expressed as $DHFR^{Nt}$ fusions under the control of the constitutive *ADH1* promoter (*ADH1pr)*. Z-scores were generated from the colony area ratio of full-length vs truncated Vrl1 baits (Figure 1F, Table S1). This identified the endosomal Rab GTPases Vps21 ($Z = 18.7$) and Ypt52 ($Z = 7.6$), and other conserved endosomal proteins including the retromer subunit Vps35 ($Z = 13$), the hydrolase receptors Vps10 ($Z = 12.9$) and Mrl1 ($Z = 7.7$), and components of the Class C Core complex Vps11 ($Z = 16.9$) and Vps18 ($Z = 12.2$; Figure 1F). Functional enrichment analysis of Vrl1 interactors ($Z > 2$) highlighted relationships with other subunits of endosomal complexes including retromer and the CORVET complex (Figure 1G, Table S2; Ashburner et al., 2000; Gene Ontology Consortium, 2021). These results suggest that Vrl1 is an endosomal SNX-BAR-like protein that contacts both membrane tethering and trafficking machinery.

Vrl1 and the Vps5 paralog Vin1 form the VINE complex

Our DHFR screen identified a strong link between Vrl1 and the uncharacterized SNX-BAR Ykr078w ($Z = 9.5$), the paralog of membrane-binding retromer subunit Vps5 (Byrne and Wolfe, 2005; Horazdovsky et al.,

130 1997), which we have named "Vrl1-Interacting Sorting Nexin 1" or Vin1 (Figure 2A). Vin1 has a reported
131 cytosolic distribution (Huh et al., 2003), which is surprising given that its paralog Vps5 localizes to
132 endosomes in a PI3P-dependent manner (Burda et al., 2002) and that Vin1 interacts with PI3P in vitro (Yu
133 and Lemmon, 2001). Increasing *VIN1* expression did not alter this cytosolic distribution pattern (Figure 2
134 S1A), suggesting that a specific condition or recruitment factor may be missing. Indeed, we found that
135 expression of *VRL1* caused a dramatic redistribution of Vin1-Envy from the cytosol to intracellular puncta
136 ($P < 0.0001$; Figure 2B and C), and that expressing *VRL1* from the strong *ADH1pr* further increased the
137 number of bright Vin1-Envy puncta ($P < 0.0001$; Figure 2 S1B and S1C). Deletion of *VIN1* prevented Vrl1-
138 Envy from forming intracellular puncta ($P < 0.001$; Figure 2B and 2C), suggesting that the localization of
139 Vrl1 and Vin1 is highly interdependent.

140 Vrl1 and Vin1 are also dependent on each other for stability, as the levels of triple hemagglutinin (3HA)
141 tagged Vrl1 and Vin1 were severely reduced in strains lacking *VIN1* or *VRL1* (17% of WT, $P < 0.001$ and
142 18% of WT, $P < 0.01$, respectively; Figure 2D and 2E). We found that Vin1-3HA strongly co-purified with
143 Vrl1-Envy (64% recovery of Vin1; Figure 2F), and Vrl1-Envy and Vin1-mScarletI (-mScI) showed a high
144 degree of colocalization at endosomal puncta (88%; Figure 2G), suggesting that these proteins form a
145 complex.

146 Since both Vin1 and Vrl1 have predicted PX domains, we wondered if, like other SNX-BARs, they bind
147 PI3P at endosomes. Vrl1 was displaced to the cytosol in a PI3K deletion mutant (*vps34*Δ, $P < 0.01$; Figure
148 2H and 2I). Since the Vrl1 PX domain is missing residues that are typically required to bind PI3P, this
149 suggests the PI3P-binding PX domain of Vin1 is important for endosomal recruitment. PI3K is activated
150 by Rab5-like GTPases (Christoforidis et al., 1999), which in turn require VPS9-domain GEFs for their
151 activity (Carney et al., 2006; Delprato and Lambright, 2007). We found that, in a *muk1*Δ*vps9*Δ strain that
152 lacks all other VPS9-domain GEFs, Vrl1 becomes dependent on its own GEF activity for localization ($P <$
153 0.001; Figure 2J and 2K), suggesting that it may leverage its ability to stimulate endosomal PI3P production
154 and promote its own membrane recruitment.

155 Taken together, our results suggest that Vrl1 and Vin1 form a novel complex that localizes to endosomes
156 in a PI3P-dependent manner (Figure 2L). Since neither Vrl1 or Vin1 are stable or capable of membrane
157 localization in the absence of the other, we reason that these proteins primarily exist as members of this
158 complex which we have named the "VPS9 GEF-Interacting Sorting Nexin" or VINE complex.

159 **Vrl1 interacts with Vin1 primarily via the AnkRD**

160 SNX-BAR proteins interact via an extensive hydrophobic interface between the BAR domains (van
161 Weering et al., 2012). The ColabFold algorithm (Mirdita et al., 2021) predicted that the PX-like and BAR

162 domains of Vrl1 (aa 732-1090) bind to the PX and BAR domains of Vin1 (aa 110-585) to form a canonical
163 SNX-BAR dimer (pTMscore = 0.75; Figure 3A). To assess the accuracy of ColabFold in predicting specific
164 BAR domain pairings, we systematically modelled pairwise homotypic and heterotypic interactions of
165 several yeast SNX-BAR proteins (Figure 3B, Table S3). This accurately predicted the homodimerization
166 of Mvp1 (Suzuki et al., 2021) and the heterodimerization of Vps5/Vps17 (Seaman and Williams, 2002).
167 Neither Vrl1 nor Vin1 were predicted to form homodimers, though unexpectedly Vrl1 was predicted to pair
168 equally well with both Vin1 and its paralog Vps5.

169 We wondered if Vrl1 could also partner with Vps5 to form a novel retromer-like complex. First, we tested
170 all known yeast SNX-BAR proteins for their ability to bind Vrl1 (Figure 3C) and found that Vin1 is the
171 only yeast SNX-BAR that binds Vrl1 at a detectable level in cell lysates. Vrl1 also failed to bind Vps5 when
172 *VIN1* was deleted (Figure 3D), and we found no evidence that Vrl1 partners with other retromer subunits
173 (Figure 3 S1A), but this assay could fail to detect weak or transient interactions. Using functional readouts,
174 we found that Vrl1 was unable to promote the endosomal localization of Vps10 (Figure 3 S1B) or Vps35
175 (Figure 3 S1C and S1D) in strains lacking Vps5 and/or Vps17, indicating that Vrl1 does not functionally
176 pair with retromer SNX-BARs and that Vin1/Vrl1 cannot replace Vps5/17 to form a retromer-like complex.
177 These results further suggest that Vrl1 has strong isoform specificity and that interactions beyond the BAR-
178 BAR interface could be responsible for its specific recognition of Vin1.

179 To identify regions critical for Vrl1-Vin1 binding, we quantified the membrane recruitment of Vin1-
180 mScarletI in cells expressing a series of Envy-tagged Vrl1 fragments (Figure 3E and 3F). We found that
181 the GEF-deficient mutant ($Vrl1^{D373A}$; Bean et al., 2015) and the N-terminal truncation ($Vrl1^{158\text{-end}}$)
182 significantly recruited Vin1 ($P < 0.0001$ and $P < 0.001$, respectively; Figure 3G) despite the weaker punctate
183 localization of the $Vrl1^{158\text{-end}}$ construct relative to WT, which could explain its reduced recruitment of Vin1.
184 Deletion of C-terminal sequences (eg $Vrl1^{1\text{-}465}$) blocked the membrane localization of both Vrl1 and Vin1.
185 To test the role of the Vrl1 PX-like and BAR domains, we replaced this region with a localization module
186 consisting of the PI3P-binding PX domain of Ypt35 fused to Envy which we refer to as "YPE" (Figure 3H).
187 Strikingly, the resulting $Vrl1(1\text{-}703)^{YPE}$ chimera strongly recruited Vin1 to puncta ($P < 0.0001$; Figure 3G),
188 suggesting that BAR-BAR interactions are dispensable for Vin1 recruitment. A further truncation that
189 removed the AnkRD to create $Vrl1(1\text{-}465)^{YPE}$ localized to endosomes yet failed to recruit Vin1 (Figure 3F
190 and 3G), indicating that the AnkRD contains a potent interacting interface for Vin1. In support of this idea,
191 the $Vrl1^{465\text{-end}}$ fragment which contains the AnkRD, PX-like and BAR domains weakly localized and
192 recruited a small but significant amount of Vin1 ($P < 0.05$) while the $Vrl1^{700\text{-end}}$ fragment containing only
193 the PX-like and BAR domains did not localize or recruit Vin1 (Figure 3F and Figure 3G).

194 We then tested the Vrl1 truncation series (Figure 3E) for the ability to CoIP Vin1-3HA (Figure 3I). We
195 found that, except for Vrl1$^{465\text{-end}}$ which weakly recruited Vin1 to membranes, all constructs that were able
196 to recruit Vin1 physically bound it by CoIP. Taken together, the Vin1 recruitment/binding assays and
197 structural predictions suggest that the VINE complex assembles primarily through an interaction between
198 Vin1 and the Vrl1 AnkRD, while a secondary interaction between the Vin1 and Vrl1 BAR domains may
199 occur at the endosomal membrane.

200 **The Vrl1 AnkRD recognizes a small region of the Vin1 N-terminus**

201 AnkRD interactions may explain how Vrl1 discriminates between Vin1 and its paralog Vps5 (Figure 3C
202 and 3D). Vin1 and Vps5 have extended, divergent N-terminal sequences preceding their respective PX
203 domains (Vin1$^{1\text{-}116}$ and Vps5$^{1\text{-}276}$; Figure 4A). When we expressed the N-terminal regions of Vin1 and Vps5
204 fused to mScarletI (Figure 4B), we observed strong recruitment of the Vin1 N-terminus by the Vrl1(1-
205 703)^{YPE} chimera, but not the YPE module alone ($P < 0.0001$; Figure 4C). In contrast, we detected no
206 recruitment of the Vps5 N-terminus by any of our tested constructs suggesting that the N-terminal regions
207 of the paralogous SNX-BARs dictate specificity for Vrl1.

208 We noticed that WT Vrl1-Envy recruited WT Vin1-mScI to colocalizing puncta, (Figure 4B) but was
209 unable to recruit the Vin1 N-terminus. The endogenous, untagged Vin1 may outcompete the Vin1 N-
210 terminal fragment for recruitment by Vrl1, however this could not be tested directly because WT Vrl1 failed
211 to localize when the Vin1 N-terminus was expressed in a *vin1*Δ strain (Figure 4 S1A and S1B). This
212 observation indicates that the Vin1 PX and BAR domains also contribute to VINE assembly and membrane
213 recruitment.

214 We generated an alignment from fungal ohnologs of Vps5 and Vin1 (Figure 4 S2A; Byrne and Wolfe,
215 2005) that identified three conserved regions in the Vin1 N-terminus (Figure 4D). When each of these
216 fragments was fused to mScarletI (Figure 4E), only region 3 (Vin1 aa 76-95) was recruited to puncta by
217 Vrl1(1-703)^{YPE} in a *vin1*Δ strain ($P < 0.05$; Figure 4F). This suggests that the Vrl1 AnkRD distinguishes
218 Vin1 from Vps5 through a short sequence in the unstructured Vin1 N-terminus.

219 **Vin1 regulates Vrl1 GEF activity via membrane localization**

220 We used different functional readouts to test if Vin1 is required for Vrl1 GEF activity. Disruption of the
221 other VPS9-domain GEF proteins results in a severe temperature sensitivity phenotype and loss of
222 endosomal PI3P (Paulsel et al., 2013; Singer-Krüger et al., 1994) that is rescued by Vrl1 in an activity-
223 dependent manner (Bean et al., 2015). We found that deletion of *VIN1,* but not *VPS5*, prevented Vrl1 from
224 rescuing the temperature sensitivity of the *muk1*Δ*vps9*Δ strain (Figure 5A). We also found that localization
225 of a fluorescent PI3P biosensor (Figure 5B) was restricted to the vacuolar membrane in *muk1*Δ*vps9*Δ*vin1*Δ

226 cells expressing Vrl1 (Figure 5C), suggesting that VINE promotes the synthesis of endosomal PI3P only
227 when fully assembled.

228 We previously found that Vrl1 recovers the PI3P-dependent endosomal localization of retromer in a
229 *muk1*Δ*vps9*Δ strain (Bean et al., 2015). By quantifying the localization of the endogenously tagged retromer
230 subunit Vps26-GFP (Figure 5D), we reproduced this finding and found that deletion of *VIN1* blocked rescue
231 ($P < 0.01$; Figure 5E). We next tested if Vin1 was still required for Vrl1 activity when the PX-like and BAR
232 domains of Vrl1 were replaced by the YPE endosomal anchor (Figure 3H) using Vps26-mScarletI
233 localization as a readout (Figure 5F). We observed that Vrl1(1-465)^{YPE} and Vrl1(1-703)^{YPE}, but not WT
234 Vrl1, fully rescued the endosomal localization of Vps26-mScarletI in a *muk1*Δ*vps9*Δ*vin1*Δ strain ($P < 0.001$;
235 Figure 5G). These results suggest that Vin1 regulates the activity of Vrl1 by promoting its localization to
236 endosomes.

237 **The VINE complex exhibits characteristics of a SNX-BAR membrane sorting complex**

238 We wondered if the VINE complex occupies endosomal membrane tubules as other SNX-BAR coat
239 complexes do (Suzuki et al., 2021; van Weering et al., 2012; Zhang et al., 2021). To test this, we co-
240 overexpressed Vrl1 and GFP-Vin1 on the strong *ADH1* and *NOP1* promoters, respectively, and acquired
241 images of GFP-Vin1 at 100ms intervals (Figure 6A). When compared to the endosomal marker Did2-
242 mRuby2, we could observe GFP-Vin1 in tubular structures that eventually underwent scission and
243 separated from the endosome (Figure 6A and 6B).

244 The budding of VINE-coated endosomal tubules suggests the VINE complex transports cargo proteins
245 from this organelle. We examined the localization of several candidates in the presence and absence of
246 Vrl1 (Figure 6C), including the mannose 6-phosphate receptor (MPR) homolog Mrl1, which had a strong
247 DHFR interaction score with Vrl1 ($Z = 7.7$; Figure 1G), and two proteins that require other SNX-BARs
248 for their transport (Seaman et al., 1998, 1997; Suzuki and Emr, 2018; Suzuki et al., 2021). We found that
249 *VRL1* expression had no significant effect on the localization of the retromer cargo Vps10 or the Snx4
250 cargo Atg27 but caused a significant decrease in the number of bright Mrl1-GFP puncta per cell (61%
251 decrease relative to *vrl1*, $P < 0.05$; Figure 6D). Vrl1 GEF activity was not required for this effect ($P <$
252 0.05; Figure 6E and 6F), indicating that Vrl1 does not alter Mrl1 distribution by influencing the local
253 activity of endosomal Rabs. Correction of the *vrl1* frameshift mutation using CRISPR-Cas9 gene editing
254 technology restored the punctate localization of Vin1 (Figure 6 S1A) and caused a similar change in Mrl1
255 localization ($P < 0.01$; Figure 6 S1B and S1C). This Vrl1-dependent change in Mrl1 distribution strongly
256 suggests that the VINE complex regulates the Mrl1 intracellular trafficking itinerary.

257 The VINE complex could sort Mrl1 by recognizing sequences in its cytosolic tail or bind another protein
258 that interacts with the MPR-like lumenal domain of Mrl1. A Vps10 mutant missing its cytoplasmic tail
259 ($Vps10^{\Delta Ct}$) lacks sorting signals and is transported to the vacuolar membrane and lumen (Bean et al.,
260 2017; Cereghino et al., 1995; Cooper and Stevens, 1996). We hypothesized that if the Mrl1 tail contains a
261 signal for VINE-mediated sorting, transplanting it onto $Vps10^{\Delta Ct}$ ($Vps10^{\Delta Ct}$-$Mrl1^{Ct}$; Figure 6G) would
262 confer VINE-dependent effects. We found that expression of *VRL1* did not alter the localization of WT
263 Vps10 or $Vps10^{\Delta Ct}$, the latter of which was targeted to the vacuolar membrane (Figure 6H). $Vps10^{\Delta Ct}$-
264 $Mrl1^{Ct}$ localized to perivacuolar puncta and the vacuolar membrane in *vrl1* cells, indicating the presence
265 of VINE-independent sorting signals in the Mrl1 tail (Figure 6H). *VRL1* expression caused a significant
266 decrease in the proportion of cells displaying punctate $Vps10^{\Delta Ct}$-$Mrl1^{Ct}$ (14% decrease relative to *vrl1*, $P <$
267 0.001; Figure 6I), suggesting that the Mrl1 cytoplasmic tail is sufficient to confer VINE complex-
268 mediated transport.

269 Because VINE redistributes Mrl1 from endosomes to the vacuolar membrane, we hypothesized that Mrl1
270 follows a Golgi-vacuole-endosome-Golgi recycling loop and that loss of Vrl1 specifically delays
271 endosome to Golgi retrograde transport. Atg27, which follows a similar itinerary, relies on Snx4 to
272 recycle it from vacuoles to the endosome (Suzuki and Emr, 2018). We observed that Mrl1-mScI was
273 mislocalized to the vacuolar membrane in a *snx4*Δ strain (Figure 6J), which caused a significant decrease
274 in endosomal Mrl1-mScI ($P < 0.0001$; Figure 6K), suggesting that Mrl1 is partially transported from the
275 vacuole to the endosome by Snx4-containing coat complexes. Taken together, these results support a
276 model where VINE enhances the recycling of the cargo protein Mrl1 at endosomes, causing a change in
277 its steady state distribution (Figure 6L).

278 Discussion

279 We have identified a novel endosomal SNX-BAR complex composed of the VPS9-domain GEF Vrl1 and
280 the Vps5 paralog Vin1 which we have named the VINE complex. Our work suggests that VINE forms a
281 novel class of endosomal transport carriers and sorts a unique set of cargo proteins that includes the
282 mannose 6-phophate receptor-like protein Mrl1.

283 Divergent N-terminal sequences in paralogous SNX-BARs specify complex formation

284 The function of the Vps5-related SNX-BAR protein Vin1 was not previously known. We found that in
285 the absence of Vrl1, Vin1 is unstable and displaced to the cytosol suggesting that it functions solely as a
286 member of the VINE complex. Vin1 and Vrl1 are both predicted to have PX-BAR domains and dimerize
287 through a canonical BAR-BAR interface, yet this interaction is not the primary driver of Vrl1-Vin1
288 association. Instead, we found that a short sequence within the unstructured N-terminal extension of Vin1

289 binds specifically to the AnkRD of Vrl1, and this is necessary for selective incorporation into the VINE
290 complex. Our work suggests that VINE assembly requires two inputs: a strong interaction involving the
291 Vin1 N-terminus and a weak interaction between the BAR domains that may occur primarily at the
292 endosomal membrane.

293 The Vin1 paralog Vps5 also has an unstructured N-terminus that is critical for its assembly with the
294 retromer complex and binds to a conserved patch on the Vps29 subunit (Collins et al., 2005; Seaman and
295 Williams, 2002). Moreover, the interaction between Vps5 and Vps17 PX-BAR domains requires
296 chemical crosslinkers to detect in detergent-solubilized lysates (Horazdovsky et al., 1997), suggesting the
297 interaction is weak or mediated largely by hydrophobic interactions. This supports a model for retromer
298 assembly that parallels that of the VINE complex, where the Vps5 N-terminus makes critical interactions
299 with other retromer subunits and drives the assembly of the Vps5-Vps17 BAR-BAR dimer through an
300 avidity effect.

301 Vin1 and Vps5 arose from a single ancestral gene during a whole-genome duplication (WGD) event
302 (Byrne and Wolfe, 2005; Wolfe and Shields, 1997), and subsequently diverged to assume new roles in the
303 VINE and retromer complexes, respectively. In pre-WGD species, the single ancestral form of Vps5 must
304 partner with both Vrl1 and Vps17, which requires some promiscuity in BAR-BAR pairing. This is
305 consistent with our ab initio modeling, which predicted a variety of pairings between the PX-BAR
306 domains of Vps5, Vps17, Vrl1 and Vin1, while the PX-BAR protein Mvp1 was predicted to form only
307 homodimers, consistent with in vivo observations (Suzuki et al., 2021).

308 Van Weering et al. (2012) have proposed a lock and key model to explain the specificity of SNX-BAR
309 pairing. In this model, paired charges within the hydrophobic BAR-BAR interface enforce the specificity
310 of BAR-BAR interactions, and loss of these charged residues results in more promiscuous BAR pairing.
311 Promiscuous BAR-BAR coupling could explain why interactions mediated by the N-termini of Vin1 and
312 Vps5 are needed to specify complex assembly.

313 New functions have been uncovered for the extended N-termini of other SNX-BAR proteins, suggesting
314 these extended regions have previously unappreciated regulatory roles. SNX1, which is the human
315 homolog of Vps5 and Vin1, recognizes SNX5 (or its homolog SNX6) through BAR-BAR interactions
316 based on lock-and-key charge pairing, and engages with other complexes, including SNX27 (Simonetti et
317 al., 2021; Yong et al., 2021) and the retromer subunit VPS29 (Swarbrick et al., 2011), through its
318 unstructured N-terminal domain. Thus, the N-termini of the SNX1/Vps5/Vin1 family of SNX-BAR
319 proteins have diversified to bind different proteins and participate in different sorting complexes.

320 **The VINE complex is both a SNX-BAR coat and a VPS9-domain GEF**

321 The VINE complex is the first described SNX-BAR coat to possess a VPS9 domain-containing subunit.
322 Retromer binds the VPS9-domain GEFs Vps9 and Muk1, which redundantly activate Rab5-like GTPases
323 to stimulate PI3P production at endosomes (Bean et al., 2015). One benefit of wiring SNX-BARs to
324 VPS9-domain GEFs could be to generate a local enrichment of PI3P that enhances SNX-BAR assembly.
325 Indeed, we find that VINE localization requires its own GEF activity in a strain lacking other VPS9-
326 domain GEFs.

327 The human Vrl1 homolog VARP also contains a VPS9 domain and associates with retromer (Hesketh et
328 al., 2014), albeit through a distinct interaction involving a motif that is not present in Vrl1 (Crawley-
329 Snowdon et al., 2020). This example of convergent evolution suggests that the linking of retromer to the
330 activation of endosomal Rabs has an important and conserved role. VARP activates Rab21, which is
331 related to Rab5 (Stenmark and Olkkonen, 2001) and interacts with PI3K in a proximity-based assay (del
332 Olmo et al., 2019), though it has not yet been shown to stimulate PI3K activity. Because endosomal Rab
333 GTPases also recruit a variety of effectors including the conserved tethering complexes Rabenosyn-
334 5/Vac1 and CORVET (Cabrera et al., 2013; Christoforidis et al., 1999; Peplowska et al., 2007; Peterson
335 et al., 1999) further work is required to clarify the conserved functional link between VPS9-domain GEFs
336 and SNX-BAR sorting complexes.

337 **VINE forms endosomal transport carriers and regulates cargo distribution**

338 Our work suggests that VINE is a novel sorting complex that acts in a pathway-specific manner, thus
339 joining the group of SNX-BAR complexes that promote independent sorting pathways from the
340 endosome or vacuole in yeast (Ma and Burd, 2020; Suzuki et al., 2021). We identified the MPR-related
341 protein Mrl1 as a candidate VINE cargo. Although the function of Mrl1 is unclear, there is evidence that
342 it works jointly with Vps10 to enhance the transport or maturation of some vacuolar proteases (Whyte and
343 Munro, 2001). Restoring VINE function alters the steady state localization of Mrl1 and could modulate
344 the rate at which it delivers proteins to the vacuole. The metabolic implications of VINE-mediated Mrl1
345 sorting and the extent to which Mrl1 uses redundant SNX-BAR trafficking pathways are important topics
346 for future study.

347 VARP, like Vrl1, also has a cargo-sorting role, as it binds to VAMP7 and cooperates with retromer to
348 direct it on an endosome to cell surface pathway (Crawley-Snowdon et al., 2020; Hesketh et al., 2014;
349 Schäfer et al., 2012). Additional research will be needed to understand the unique functions of the VINE
350 complex in protein sorting and clarify its functional conservation with VARP. Importantly, almost all
351 studies on endosomal trafficking and signaling have been performed in strains that lack the VINE
352 complex, and we anticipate that many other VINE cargos exist. Some proteins that are recycled by SNX-

353 BAR-dependent pathways, such as phospholipid flippases, are themselves important for organelle
354 function or signaling (Dalton et al., 2017; Liu et al., 2008). In the absence of functional VINE, such
355 proteins may be missorted and/or have altered properties. Restoring VINE may therefore restore cellular
356 processes and reveal new biology.
357

358 ## Materials and Methods

359 **Yeast strains and plasmids**

360 Yeast strains and plasmids used in this study are described in Tables S4 and S5, respectively. Yeast strains
361 were built in the BY4741 strain background using homologous recombination-based integration unless
362 otherwise indicated. Gene deletions, promoter exchanges and tags were confirmed by colony PCR and
363 either western blot or fluorescence microscopy where possible. Plasmids were built by homologous
364 recombination in yeast, recovered in *Escherichia coli* and confirmed by sequencing.

365 **Bioinformatic analysis of protein folding and sequence conservation**

366 Prediction of protein structure and binding interfaces was performed using Phyre2 (Kelley et al., 2015) and
367 the ColabFold advanced server (Mirdita et al., 2021) with default settings. Vrl1 amino acid sequences were
368 from the *S. cerevisiae* strain RM11-1a. Orthologous sequences were obtained from the OrthoDB database
369 (Kriventseva et al., 2019), aligned using the EMBL-EBI Multiple Sequence Comparison by Log-
370 Expectation (MUSCLE) tool (https://www.ebi.ac.uk/Tools/msa/muscle) and presented using Jalview
371 (http://www.jalview.org).

372 **DHFR protein fragment complementation assay and ontology analysis**

373 A MATa strain containing a plasmid that expresses the Vrl1-DHFR[1,2] ($DHFR^{Nt}$) fusion from the *ADH1*
374 promoter, or the p*ADHpr-VRL1(1-465)-DHFR*^{Nt} control, was crossed into a library of MATα strains (n = ~
375 4,300) expressing proteins fused to DHFR[3] ($DHFR^{Ct}$; Tarassov et al., 2008). Diploids were subjected to
376 two rounds of double mutant selection followed by two rounds of selection on media containing 200 µg/ml
377 methotrexate, in 1536 arrays. Manipulations were carried out using a BM3-BC pinning robot (S&P
378 Robotics inc., Toronto, Canada). Colony area was analyzed using CellProfiler (Lamprecht et al., 2007) after
379 8 days at 30 °C. Z-scores were generated using median colony area from two technical replicates for each
380 Vrl1-prey combination. Functional analysis of Vrl1 DHFR interactors (Z > 2) was performed using the
381 Gene Ontology (Ashburner et al., 2000; Gene Ontology Consortium, 2021) GO Enrichment Analysis tool
382 (Mi et al., 2019).

383 **Fluorescence microscopy and automated image analysis**

384 Yeast cells were diluted from overnight cultures in fresh synthetic dextrose-based media (SD) and incubated
385 at 30 °C for ~4 hours or until they reached an optical density of ~ 0.4 - 0.7 OD_{600} unless otherwise indicated.

386 Log phase yeast were transferred to concanavalin A-treated 96-well glass bottom plates (Eppendorf,
387 Hamburg, Germany) and imaged using a DMi8 microscope (Leica Microsystems, Wetzlar, Germany)
388 equipped with an ORCA-flash 4.0 digital camera (Hamamatsu Photonics, Shizuoka, Japan) and a high-
389 contrast Plan-Apochromat 63x/1.30 Glyc CORR CS oil immersion lens (Leica Microsystems, Wetzlar,
390 Germany). Image acquisition and processing was performed using the MetaMorph 7.8 software package
391 (MDS Analytical Technologies, Sunnyvale, California). Yeast vacuoles were labelled with 100 µM CMAC
392 (Setareh, San Jose, California) or 4 µM FM4-64 (Life Technologies, Carlsbad, California) for 30 minutes
393 at 30 °C. Dye-treated cells were washed once in SD media prior to imaging.

394 Linear intensity scale changes were uniformly applied to all images in an experimental set using
395 MetaMorph 7.8 (MDS Analytical Technologies, Sunnyvale, California). Images were prepared for
396 presentation using Photoshop CC 2020 (Adobe, San Jose, California) and Illustrator CC 2020 (Adobe, San
397 Jose, California). Quantification was performed on unscaled raw imaged with scripted MetaMorph 7.8
398 journals (MDS Analytical Technologies, Sunnyvale, California). The Count Nuclei feature was used to
399 filter out dead cells and identify live cells based on intensity about local background (IALB). The
400 Granularity feature was used to identify puncta in a dead cell-masked intermediate image based on IALB.
401 Masking functions were performed using the Arithmetic function with Logical AND.

402 **Coimmunoprecipitation, western blotting and spheroplasting**

403 For western blot-based stability assays, yeast cells were grown to log phase in SD media at 30 °C and 10
404 OD_{600}/ml equivalents of cells were harvested and stored at -80 °C. Cells were thawed and lysed by vortexing
405 in 100 µl of Thorner buffer (8 M Urea, 5% SDS, 40mM Tris-Cl (pH 6.4), 1% beta-mercaptoethanol and
406 0.4 mg/ml bromophenol blue) with ~100 µl of acid-washed glass beads/sample at 70 °C for 5 minutes.
407 Lysates were centrifuged at 14,000 RPM for 30 seconds and separated on 8% SDS-PAGE gels followed by
408 western blotting with mouse anti-HA (H9658, Clone HA-7, MilliporeSigma) or anti-PGK1 monoclonal
409 antibodies (AB_2532235, 22C5D8, Invitrogen), and secondary polyclonal goat anti-mouse antibodies
410 conjugated to horseradish peroxidase (115–035-146; Jackson ImmunoResearch Laboratories).

411 For CoIPs, yeast cells were grown to log phase in SD media at 30 °C and 75 OD_{600}/ml equivalents of cells
412 were incubated in 50 mM Tris-Cl with 10 mM DTT (pH 9.5) for 15 minutes at room temperature and
413 digested in spheroplasting buffer (1.2 M sorbitol, 50 mM KH_2PO_4, 1 mM $MgCl_2$ and 250 µg/ml zymolase
414 at pH 7.4) at 30 °C for 1 hour. Spheroplasts were washed twice with 1.2 M sorbitol, frozen at -80 °C, then
415 incubated in 500 µl of lysis buffer (0.1% Tween-20, 50 mM HEPES, 1 mM EDTA, 50 mM NaCl, 1 mM
416 PMSF and 1x fungal ProteaseArrest, pH 7.4) at room temperature for 10 minutes. 50 µl volumes of lysate
417 were collected for each sample and mixed with 2x Laemmli buffer (4% SDS, 20% glycerol, 120 mM Tris-
418 Cl (pH 6.8), 0.01g bromophenol blue and 10% beta-mercaptoethanol) for western analysis while remaining

419 lysates were incubated with either a polyclonal rabbit anti-GFP (EU2, Eusera) or a polyclonal rabbit anti-
420 HA antibody (ab9110, Abcam) at 4 °C for 1 hour. Antibody-treated samples were next incubated with
421 Protein A-Sepharose beads (GE Healthcare) at 4 °C for 1 hour. Beads were washed 3x in lysis buffer before
422 being resuspended in 50 µl of Thorner buffer and heated at 80 °C for 5 minutes. Western blotting of proteins
423 separated on 8% SDS-PAGE gels was carried out with monoclonal mouse anti-HA (H9658, Clone HA-7,
424 MilliporeSigma), monoclonal mouse anti-HA (MMS-101R; Covance) or monoclonal mouse anti-GFP
425 antibodies (11–814–460-001; Roche) prior to secondary antibody treatment with polyclonal goat anti-
426 mouse conjugated to horseradish peroxidase (115–035-146; Jackson ImmunoResearch Laboratories). Blots
427 were developed with Amersham ECL (RPN2232, Cytiva) or Amersham ECL Prime (RPN2236, Cytiva)
428 chemiluminescent western blot detection reagents and exposed using Amersham Hyperfilm ECL (GE
429 Healthcare). Densitometry of scanned films was performed using ImageJ (Schneider et al., 2012).

430 **Correction of genomic *vrl1* mutation using CRISPR-Cas9**

431 A plasmid containing the Cas9 enzyme and a single guide RNA (sgRNA) targeting the *VRL1*-disrupting
432 *yml003w* mutation was pre-cloned using small fragment golden gate assembly (Marillonnet and Grützner,
433 2020). BY4741 was co-transformed with linearized split *URA3* marker Cas9-sgRNA(*VRL1*) plasmid and
434 PCR product containing the corrected *VRL1* sequence. Ura^+ colonies were sequenced and an isolate with
435 intact *VRL1* was frozen down and used for experiments.

436 **Statistical analysis of quantitative data**

437 Statistical tests were performed using GraphPad Prism 9.1.0 (GraphPad Software, San. Diego, California)
438 as indicated in figure legends with the appropriate post-hoc tests. Normality of data was assumed but not
439 formally tested and hypotheses were measured against a threshold of 95% confidence (or $P < 0.05$). Graphs
440 were made in Microsoft Excel 2019 (Microsoft, Redmond, Washington). Column charts represent the
441 average value from biological replicates while scatter points represent data from individual replicates and
442 are coloured by replicate. Error bars report the standard error of the mean value.
443

444 **Acknowledgements**

445 We thank Dr. Christian Landry (Laval University, Quebec City, Canada) and Dr. Maya Schuldiner
446 (Weizmann Institute of Science, Rehovot, Israel) for sharing yeast libraries, Drs. Bjorn Bean and Vincent
447 Martin (Concordia University, Montreal, Canada) for sharing yeast CRISPR reagents and Dr. Luc
448 Berthiaume (University of Alberta, Edmonton, Canada) for generously sharing rabbit anti-GFP serum.

449 We gratefully acknowledge funding support from the Natural Sciences and Engineering Research Council
450 of Canada (grant 2016-04290 to EC and PGS-D3 Doctoral Scholarship to SPS); Canada Foundation for
451 Innovation (Leading Edge Fund 30636); Canadian Institutes of Health Research (grants 247169 and 365914

452 to EC, CGS-M Frederick Banting and Charles Best Canada Graduate Scholarship to SPS and MSF); BC
453 Children's Hospital Research Institute Jan M. Friedman Graduate Studentship to SPS; University of British
454 Columbia Catalyst Paper Corporation Affiliated Fellowship and 4-Year Doctoral Fellowship to SPS and
455 University of British Columbia Medical Genetics Rotation Award to MSF.
456

457 **Author Contributions**

458 Conceptualization, EC; Methodology, SPS, MSF and EC; Validation, SPS and MSF; Formal analysis, SPS
459 and MSF; Investigation, SPS, MSF and MD; Resources, SPS, MSF and MD; Data curation, SPS and MSF;
460 Writing – original draft, SPS and MSF; Writing – review & editing, SPS, MSF and EC; Visualization, SPS
461 and MSF; Supervision, SPS and EC; Project administration, EC; Funding acquisition, EC.
462

463 **Conflict of Interest Statement**

464 The authors declare that there are no conflicts of interest.
465

466 **References**

467 Arlt H, Reggiori F, Ungermann C. 2015. Retromer and the dynamin Vps1 cooperate in the retrieval of
468 transmembrane proteins from vacuoles. J. Cell Sci. *128(4)*, 645–55.

469 Ashburner M, Ball CA, Blake JA, Botstein D, Butler H, Cherry JM, Davis AP, Dolinski K, Dwight SS,
470 Eppig JT, Harris MA, Hill DP, Issel-Tarver L, Kasarskis A, Lewis S, Matese JC, Richardson JE, Ringwald
471 M, Rubin GM, Sherlock G. 2000. Gene ontology: Tool for the unification of biology. Nat. Genet. *25(1)*,
472 25–9.

473 Barr F, Lambright DG. 2010. Rab GEFs and GAPs. Curr. Opin. Cell. Biol. *22(4)*, 461–70.

474 Bean BDM, Davey M, Conibear E. 2017. Cargo selectivity of yeast sorting nexins. Traffic *18(2)*, 110–122.

475 Bean BDM, Davey M, Snider J, Jessulat M, Deineko V, Tinney M, Stagljar I, Babu M, Conibear E. 2015.
476 Rab5-family guanine nucleotide exchange factors bind retromer and promote its recruitment to endosomes.
477 Mol. Biol. Cell *26(6)*, 1119–28.

478 Burd C, Cullen PJ. 2014. Retromer: A master conductor of endosome sorting. Cold Spring Harb. Perspect.
479 Biol. *6(2)*, a016774

480 Burda P, Padilla SM, Sarkar S, Emr SD. 2002. Retromer function in endosome-to-Golgi retrograde
481 transport is regulated by the yeast Vps34 PtdIns 3-kinase. J. Cell Sci. *115(20),* 3889–3900.

482 Byrne KP, Wolfe KH. 2005. The Yeast Gene Order Browser: combining curated homology and syntenic
483 context reveals gene fate in polyploid species. *Genome Res. 15(10),* 1456–61.

484 Cabrera M, Arlt H, Epp N, Lachmann J, Griffith J, Perz A, Reggiori F, Ungermann C. 2013. Functional
485 separation of endosomal fusion factors and the class C core vacuole/endosome tethering (CORVET)
486 complex in endosome biogenesis. J. Biol. Chem. *288(7)*, 5166-75.

487 Carlton J, Bujny M, Rutherford A, Cullen P. 2005. Sorting nexins – unifying trends and new perspectives.
488 Traffic *6(2),* 75–82.

489 Carney DS, Davies BA, Horazdovsky BF. 2006. Vps9 domain-containing proteins: Activators of Rab5
490 GTPases from yeast to neurons. Trends Cell Biol. *16(1)*, 27–35.

491 Cereghino JL, Marcusson EG, Emr SD. 1995. The cytoplasmic tail domain of the vacuolar protein sorting
492 receptor Vps10p and a subset of VPS gene products regulate receptor stability, function, and localization.
493 Mol. Biol. Cell *6(9)*, 1089–102.

494 Cheever ML, Sato TK, de Beer T, Kutateladze TG, Emr SD, Overduin M. 2001. Phox domain interaction
495 with PtdIns(3)P targets the Vam7 t-SNARE to vacuole membranes. *Nat. Cell Biol. 3(7)*, 613–8.

496 Christoforidis S, Miaczynska M, Ashman K, Wilm M, Zhao L, Yip SC, Waterfield MD, Backer JM, Zerial
497 M. 1999. Phosphatidylinositol-3-OH kinases are Rab5 effectors. Nat. Cell Biol. *1(4)*, 249–52.

498 Collins BM, Skinner CF, Watson PJ, Seaman MNJ, Owen DJ. 2005. Vps29 has a phosphoesterase fold that
499 acts as a protein interaction scaffold for retromer assembly. Nat. Struct. Mol. Biol. *12(7)*, 594–602.

500 Cooper AA, Stevens TH. 1996. Vps10p cycles between the late-Golgi and prevacuolar compartments in its
501 function as the sorting receptor for multiple yeast vacuolar hydrolases. J. Cell Biol. *133(3)*, 529–41.

502 Crawley-Snowdon H, Yang J-C, Zaccai NR, Davis LJ, Wartosch L, Herman EK, Bright NA, Swarbrick JS,
503 Collins BM, Jackson LP, Seaman MNJ, Luzio JP, Dacks JB, Neuhaus D, Owen DJ. 2020. Mechanism and
504 evolution of the Zn-fingernail required for interaction of VARP with VPS29. Nat. Commun. *2020 11(1)*,
505 5031.

506 Cullen PJ, Korswagen HC. 2012. Sorting nexins provide diversity for retromer-dependent trafficking
507 events. Nat. Cell Biol. *14(1)*, 29–37.

508 Dalton LE, Bean BDM, Davey M, Conibear E. 2017. Quantitative high-content imaging identifies novel
509 regulators of Neo1 trafficking at endosomes. Mol. Biol. Cell *28(11)*, 1539–50.

510 del Olmo T, Lauzier A, Normandin C, Larcher R, Lecours M, Jean D, Lessard L, Steinberg F, Boisvert F,
511 Jean S. 2019. APEX2-mediated RAB proximity labeling identifies a role for RAB21 in clathrin-
512 independent cargo sorting. EMBO Rep. *20*, e47192.

513 Delprato A, Lambright DG. 2007. Structural basis for Rab GTPase activation by VPS9 domain exchange
514 factors. Nat. Struct. Mol. Biol. *14(5)*, 406–12.

515 Frost A, Unger VM, de Camilli P. 2009. The BAR domain superfamily: membrane-molding
516 macromolecules. Cell *137(2)*, 191–6.

517 Gallon M, Cullen PJ. 2015. Retromer and sorting nexins in endosomal sorting. Biochem. Soc. Trans. *43(1)*,
518 33–47.

519 Hama H, Tall GG, Horazdovsky BF. 1999. Vps9p is a guanine nucleotide exchange factor involved in
520 vesicle- mediated vacuolar protein transport. J. Biol. Chem. *274(21)*, 15284–91.

521 Hesketh GG, Pérez-Dorado I, Jackson LP, Wartosch L, Schäfer IB, Gray SR, McCoy AJ, Zeldin OB,
522 Garman EF, Harbour ME, Evans PR, Seaman MNJ, Luzio JP, Owen DJ. 2014. VARP is recruited on to
523 endosomes by direct interaction with retromer, where together they function in export to the cell surface.
524 Dev. Cell *29(5)*, 591–606.

525 Hettema EH, Lewis MJ, Black MW, Pelham HRB. 2003. Retromer and the sorting nexins Snx4/41/42
526 mediate distinct retrieval pathways from yeast endosomes. EMBO J. *22(3),* 548–57.

527 Hong W. 2019. SNXs take center stage in endosomal sorting. Nat. Cell Biol. *21(10)*, 1175–7.

528 Horazdovsky BF, Davies BA, Seaman MNJ, McLaughlin SA, Yoon SH, Emr SD. 1997. A sorting nexin-1
529 homologue, Vps5p, forms a complex with Vps17p and is required for recycling the vacuolar protein-sorting
530 receptor. Mol. Biol. Cell *8(8*), 1529–41.

531 Huh W-K, Falvo JV., Gerke LC, Carroll AS, Howson RW, Weissman JS, O'Shea EK. 2003. Global analysis
532 of protein localization in budding yeast. Nature *425(6959)*, 686–91.

533 Jahn R, Scheller RH. 2006. SNAREs – engines for membrane fusion. Nat. Rev. Mol. Cell Biol. *7(9)*, 631–
534 43.

535 Kelley LA, Mezulis S, Yates CM, Wass MN, Sternberg MJE. 2015. The Phyre2 web portal for protein
536 modeling, prediction and analysis. Nat. Protoc. *10(6)*, 845–58.

537 Kriventseva EV, Kuznetsov D, Tegenfeldt F, Manni M, Dias R, Simão FA, Zdobnov EM. 2019. OrthoDB
538 v10: sampling the diversity of animal, plant, fungal, protist, bacterial and viral genomes for evolutionary
539 and functional annotations of orthologs. Nucleic Acids Res. *47(D1)*, D807–11.

540 Lamprecht MR, Sabatini DM, Carpenter AE. 2007. CellProfiler: free, versatile software for automated
541 biological image analysis. BioTechniques *42(1)*, 71–5.

542 Liu K, Surendhran K, Nothwehr SF, Graham TR. 2008. P4-ATPase Requirement for AP-1/Clathrin
543 Function in Protein Transport from the trans-Golgi Network and Early Endosomes. Mol. Biol. Cell *19(8),*
544 3526–35.

545 Ma M, Burd CG. 2020. Retrograde trafficking and plasma membrane recycling pathways of the budding
546 yeast Saccharomyces cerevisiae. Traffic *21(1)*, 45–59.

547 Marillonnet S, Grützner R. 2020. Synthetic DNA Assembly Using Golden Gate Cloning and the
548 Hierarchical Modular Cloning Pipeline. Curr. Protoc. Mol. Biol. *130(1)*, e115.

549 Mi H, Muruganujan A, Ebert D, Huang X, Thomas PD. 2019. PANTHER version 14: More genomes, a
550 new PANTHER GO-slim and improvements in enrichment analysis tools. Nucleic Acids Res. *47(D1)*,
551 D419–26.

552 Michnick SW, Ear PH, Landry C, Malleshaiah MK, Messier V. 2010. A toolkit of protein-fragment
553 complementation assays for studying and dissecting large-scale and dynamic protein-protein interactions
554 in living cells. Methods Enzymol. *470*, 335–68.

555 Mirdita M, Ovchinnikov S, Steinegger M. 2021. ColabFold - Making protein folding accessible to all.
556 bioRxiv 2021.08.15.456425.

557 Mohan M, Mellick GD. 2017. Role of the VPS35 D620N mutation in Parkinson's disease. Parkinsonism
558 Relat. Disord. *36*, 10–8.

559 Numrich J, Ungermann C. 2014. Endocytic Rabs in membrane trafficking and signaling. Biol. Chem.
560 *395(3)*, 327–33.

561 Paulsel AL, Merz AJ, Nickerson DP. 2013. Vps9 family protein Muk1 Is the second rab5 guanosine
562 nucleotide exchange factor in budding yeast. J. Biol. Chem. *288(25)*, 18162–71.

563 Peplowska K, Markgraf DF, Ostrowicz CW, Bange G, Ungermann C. 2007. The CORVET Tethering
564 Complex Interacts with the Yeast Rab5 Homolog Vps21 and Is Involved in Endo-Lysosomal Biogenesis.
565 Dev. Cell *12(5)*, 739–50.

566 Peterson MR, Burd CG, Emr SD. 1999. Vac1p coordinates Rab and phosphatidylinositol 3-kinase signaling
567 in Vps45p-dependent vesicle docking/fusion at the endosome. Curr. Biol. *9(3)*, 159–62.

568 Pfeffer SR. 2017. Rab GTPases: Master regulators that establish the secretory and endocytic pathways.
569 Mol. Biol. Cell *28(6)*, 712–5.

570 Rahman AA, Morrison BE. 2019. Contributions of VPS35 Mutations to Parkinson's Disease.
571 Neuroscience. *401*, 1–10.

572 Schäfer IB, Hesketh GG, Bright NA, Gray SR, Pryor PR, Evans PR, Luzio JP, Owen DJ. 2012. The binding
573 of Varp to VAMP7 traps VAMP7 in a closed, fusogenically inactive conformation. Nat. Struct. Mol. Biol.
574 *19(12)*, 1300–9.

575 Schneider CA, Rasband WS, Eliceiri KW. 2012. NIH Image to ImageJ: 25 years of image analysis. Nat.
576 Methods *9(7)*, 671–5.

577 Seaman MNJ, Williams HP. 2002. Identification of the functional domains of yeast sorting nexins Vps5p
578 and Vps17p. Mol. Biol. Cell *13(8),* 2826–40.

579 Seaman MNJ, Marcusson EG, Cereghino JL, Emr SD. 1997. Endosome to Golgi Retrieval of the Vacuolar
580 Protein Sorting Receptor, Vps10p, Requires the Function of the VPS29, VPS30, and VPS35 Gene Products.
581 J. Cell Biol. *137(1)*, 79–92.

582 Seaman MNJ, McCaffery JM, Emr SD. 1998. A membrane coat complex essential for endosome-to-Golgi
583 retrograde transport in yeast. J. Cell Biol. *142(3),* 665–81.

584 Simonetti B, Guo Q, Gimenez-Andres M, Chen K-E, Moody ERR, Evans AJ, Danson CM, Williams TA,
585 Collins BM, Cullen PJ. 2021. Mechanistic basis for SNX27-Retromer coupling to ESCPE-1 in promoting
586 endosomal cargo recycling. bioRxiv 2021.08.28.457928.

587 Singer-Krüger B, Stenmark H, Düsterhöft A, Philippsen P, Yoo JS, Gallwitz D, Zerial M. 1994. Role of
588 three rab5-like GTPases, Ypt51p, Ypt52p, and Ypt53p, in the endocytic and vacuolar protein sorting
589 pathways of yeast. J. Cell Biol. *125(2)*, 283–98.

590 Stenmark H. 2009. Rab GTPases as coordinators of vesicle traffic. Nat. Rev. Mol. Cell Biol. *10(8),* 513–
591 25.

592 Stenmark H, Olkkonen VM. 2001. The Rab GTPase family. Genome Biol. *2(5)*, reviews3007.1

593 Suzuki SW, Emr SD. 2018. Membrane protein recycling from the vacuole/lysosome membrane. J. Cell
594 Biol. *217(5),* 1623–32.

595 Suzuki SW, Oishi A, Nikulin N, Jorgensen JR, Baile MG, Emr SD. 2021. A PX-BAR protein Mvp1/SNX8
596 and a dynamin-like GTPase Vps1 drive endosomal recycling. eLife *10*, e69883.

597 Swarbrick JD, Shaw DJ, Chhabra S, Ghai R, Valkov E, Norwood SJ, Seaman MNJ, Collins BM. 2011.
598 VPS29 is not an active metallo-phosphatase but is a rigid scaffold required for retromer interaction with
599 accessory proteins. PLoS ONE *6(5)*, e20420.

600 Tarassov K, Messier V, Landry CR, Radinovic S, Serna Molina MM, Shames I, Malitskaya Y, Vogel J,
601 Bussey H, Michnick SW. 2008. An in vivo map of the yeast protein interactome. Science *320(5882),* 1465–
602 70.

603 Gene Ontology Consortium. 2021. The Gene Ontology resource: enriching a GOld mine. Nucleic Acids
604 Res. *49(D1),* D325–34.

605 van Weering JRT, Sessions RB, Traer CJ, Kloer DP, Bhatia VK, Stamou D, Carlsson SR, Hurley JH, Cullen
606 PJ. 2012. Molecular basis for SNX-BAR-mediated assembly of distinct endosomal sorting tubules. EMBO
607 J. *31(23),* 4466–83.

608 van Weering JRT, Verkade P, Cullen PJ. 2010. SNX-BAR proteins in phosphoinositide-mediated, tubular-
609 based endosomal sorting. Semin. Cell Dev. Biol. *21(4)*, 371–80.

610 Vilariño-Güell C, Wider C, Ross OA, Dachsel JC, Kachergus JM, Lincoln SJ, Soto-Ortolaza AI, Cobb SA,
611 Wilhoite GJ, Bacon JA, Bahareh Behrouz, Melrose HL, Hentati E, Puschmann A, Evans DM, Conibear E,
612 Wasserman WW, Aasly JO, Burkhard PR, Djaldetti R, Ghika J, Hentati F, Krygowska-Wajs A, Lynch T,
613 Melamed E, Rajput A, Rajput AH, Solida A, Wu RM, Uitti RJ, Wszolek ZK, Vingerhoets F, Farrer MJ.
614 2011. VPS35 mutations in parkinson disease. Am. J. Hum. Genet. *89(1),* 162–7.

615 Wen L, Tang FL, Hong Y, Luo SW, Wang CL, He W, Shen C, Jung JU, Xiong F, Lee D hoon, Zhang QG,
616 Brann D, Kim TW, Yan R, Mei L, Xiong WC. 2011. VPS35 haploinsufficiency increases Alzheimer's
617 disease neuropathology. J. Cell Biol. *195(5)*, 765–79.

618 Whyte JR, Munro S. 2001. A yeast homolog of the mammalian mannose 6-phosphate receptors contributes
619 to the sorting of vacuolar hydrolases. Curr. Biol. *11(13),* 1074–8.

620 Wolfe KH, Shields DC. 1997. Molecular evidence for an ancient duplication of the entire yeast genome.
621 Nature *387(6634)*, 708–13.

622 Xu Y, Seet LF, Hanson B, Hong W. 2001. The Phox homology (PX) domain, a new player in
623 phosphoinositide signalling. Biochem. J. *360*, 513–30.

624 Yong X, Zhao L, Hu W, Sun Q, Ham H, Liu Z, Ren J, Zhang Z, Zhou Y, Yang Q, Mo X, Hu J, Billadeau
625 DD, Jia D. 2021. SNX27-FERM-SNX1 complex structure rationalizes divergent trafficking pathways by
626 SNX17 and SNX27. Proc. Natl. Acad. Sci. U. S. A. *118(36)*, e2105510118.

627 Yu JW, Lemmon MA. 2001. All Phox Homology (PX) Domains from Saccharomyces cerevisiae
628 Specifically Recognize Phosphatidylinositol 3-Phosphate. J. Biol. Chem. *276(47),* 44179–84.

629 Zhang Y, Pang X, Li J, Xu J, Hsu VW, Sun F. 2021. Structural insights into membrane remodeling by
630 SNX1. Proc. Natl. Acad. Sci. U. S. A. *118(10)*, e2022614118.

631 Zimprich A, Benet-Pagès A, Struhal W, Graf E, Eck SH, Offman MN, Haubenberger D, Spielberger S,
632 Schulte EC, Lichtner P, Rossle SC, Klopp N, Wolf E, Seppi K, Pirker W, Presslauer S, Mollenhauer B,
633 Katzenschlager R, Foki T, Hotzy C, Reinthaler E, Harutyunyan A, Kralovics R, Peters A, Zimprich F,
634 Brücke T, Poewe W, Auff E, Trenkwalder C, Rost B, Ransmayr G, Winkelmann J, Meitinger T, Strom TM.
635 2011. A mutation in VPS35, encoding a subunit of the retromer complex, causes late-onset parkinson
636 disease. Am. J. Hum. Genet. *89(1),* 168–75.

637

638 **Figure Legends**

639 **Figure 1. Vrl1 is a predicted PX-BAR protein that interacts with conserved machinery at the**
640 **endosome.** (A) Schematic of Vrl1 and VARP domain architecture. (B) ColabFold predicts the Vrl1 C-
641 terminus has a SNX-BAR-like PX and BAR domain fold. (C) Vrl1-Envy colocalizes with Did2-mRuby2-
642 labeled endosomes, but not with the Sec7-dsRed Golgi marker. (D) Quantification of colocalization as the
643 percentage of Vrl1 puncta over RFP puncta. Two-tailed equal variance *t* test; $n = 3$, cells/strain/replicate ≥
644 1,395; **** = $P < 0.0001$. (E) Schematic of DHFR proximity screen methodology. (F) Z-score distribution
645 of the ratio of colony areas from genome-wide DHFR screens of full length and N-terminal Vrl1 baits. (G)
646 Gene Ontology (GO) functional enrichment analysis of Vrl1 DHFR interactors (Z-score > 2;
647 http://geneontology.org). GO terms of the most specific hierarchical subclass with a fold enrichment value
648 > 25 are presented as the negative base 10 log of the associated P-value from a Bonferroni-corrected

649 binomial test of significance. Scale bars, 2 µm. Error bars report standard error of the mean (SEM). Enrich.,
650 enrichment. aa, amino acids.

651 **Figure 2. Vrl1 and the Vps5 paralog Vin1 form the VINE complex.** (A) Schematic of Ykr078w (Vin1)
652 and its paralog Vps5. (B) Vin1-Envy and Vrl1-Envy require Vrl1 and Vin1, respectively, for localization
653 to puncta. (C) Quantification of Vin1-Envy and Vrl1-Envy puncta per cell. Two tailed equal variance *t*
654 tests; $n = 3$, cells/strain/replicate ≥ 1,879; *** = $P < 0.001$, **** = $P < 0.0001$. (D) Vrl1-3HA and Vin1-
655 3HA require Vin1 and Vrl1, respectively, for protein stability by western blot. Pgk1 serves as a loading
656 control. (E) Quantification of Vrl1-3HA and Vin1-3HA levels by densitometry. Two tailed Welch's *t* tests;
657 $n = 3$, ** = $P < 0.01$, *** = $P < 0.001$. (F) Co-immunoprecipitation (CoIP) of Vin1-3HA with Vrl1-Envy
658 suggests stable complex formation. (G) Vrl1-Envy colocalizes with Vin1-mScI at perivacuolar puncta. (H)
659 Vrl1-Envy requires the PI3K catalytic subunit Vps34 for punctate localization. (I) Quantification of Vrl1-
660 Envy puncta per cell. Two-tailed equal variance *t* test; $n = 3$, cells/strain/replicate ≥ 897; ** = $P < 0.01$. (J)
661 Vrl1-Envy localization in the absence of VPS9-domain GEFs is dependent on Vrl1 activity. (K)
662 Quantification of Vrl1-Envy puncta per cell. One-way ANOVA with Tukey's multiple comparison test; n
663 = 3, cells/strain/replicate ≥ 1,705; not significant, n.s. = $P > 0.05$, * = $P < 0.05$, *** = $P < 0.001$, **** = P
664 < 0.0001. (L) model of the Vin1 and Vrl1-containing VINE complex at endosomes. Scale bars, 2 µm. Error
665 bars report SEM. Exp., Exposure

666 **Figure 3. Vrl1 interacts with Vin1 primarily through the AnkRD.** (A) ColabFold-predicted physical
667 interaction of Vrl1 and Vin1 BAR domains along the canonical BAR-BAR dimerization interface.
668 pTMscore = 0.75. (B) Matrix of ColabFold-predicted BAR-BAR dimers for selected yeast SNX-BARs.
669 Hierarchical clustering was performed using an uncentered Pearson correlation with average linkage. (C)
670 Vin1 is the only yeast SNX-BAR that interacts with overexpressed Vrl1-3HA by CoIP. (D) Vin1 does not
671 compete with Vps5 for shared binding to Vrl1. (E) Schematic of Envy-tagged Vrl1 truncations and chimeras
672 in (F). (F) The Vrl1 AnkRD is necessary to recruit Vin1-mScI to puncta. Insets are scaled to match other
673 regions in the same channel. (G) Quantification of Vin1-mScI puncta per cell. One-way ANOVA with
674 Dunnett's multiple comparison test; $n = 3$, cells/strain/replicate ≥ 764; not significant, n.s. = $P > 0.05$, * =
675 $P < 0.05$, ** = $P < 0.01$, *** = $P < 0.001$, **** = $P < 0.0001$. (H) Illustration of chimeric Vrl1 fusion
676 proteins that are artificially recruited to the endosomal system by the PX domain of sorting nexin Ypt35.
677 (I) The Vrl1 AnkRD is necessary for physical interaction with Vin1-3HA by CoIP. Pgk1 serves as a loading
678 control. Scale bars, 2 µm. Error bars report SEM. OE, overexpressed. YPE, Ypt35(PX)-Envy.

679 **Figure 4. The Vrl1 AnkRD recognizes a small region of the Vin1 N-terminus.** (A) Schematic of
680 constructs used in (B, C) (B) The AnkRD-containing Vrl1-YPE chimera recruits the N-terminus of Vin1,
681 but not Vps5. Insets are scaled to match other regions in the same channel. (C) Quantification of RFP puncta

682 per cell. One-way ANOVA with Tukey's multiple comparison test; n = 3, cells/strain/replicate ≥ 902; not
683 significant, n.s. = P > 0.05, ** = P < 0.01, *** = P < 0.001, **** = P < 0.0001. (D) Schematic of Vin1 N-
684 terminal fragments used to map the Vrl1 recruitment site. (E) The AnkRD-containing Vrl1-YPE chimera
685 recruits a small fragment of the Vin1 N-terminus. Insets are scaled to match other regions in the same
686 channel. (F) Quantification of Vin1-mScI puncta per cell. Two-tailed equal variance t tests; n = 3,
687 cells/strain/replicate ≥ 294; not significant, n.s. = P > 0.05, * = P < 0.05, ** = P < 0.01. Scale bars, 2 µm.
688 Error bars report SEM. OE, overexpressed. FL, full length.

689 **Figure 5. Vin1 controls Vrl1 GEF activity via membrane localization.** (A) Deletion of *VIN1*, but not
690 *VPS5*, prevents Vrl1 from rescuing the temperature sensitivity of a strain lacking other VPS9-domain GEFs.
691 (B) Schematic of PI3P-binding fluorescent biosensor. (C) Deletion of *VIN1* prevents Vrl1 from stimulating
692 endosomal PI3P production in a strain lacking other VPS9-domain GEFs. (D) Deletion of *VIN1* prevents
693 Vrl1 from rescuing Vps26-GFP localization in a strain lacking other VPS9-domain GEFs. (E)
694 Quantification of Vps26-GFP puncta per cell. One-way ANOVA with Tukey's multiple comparison test; n
695 = 3, cells/strain/replicate ≥ 1,503; not significant, n.s. = P > 0.05, * = P < 0.05, ** = P < 0.01, *** = P <
696 0.001. (F) Vin1 is dispensable for Vrl1 activity when fragments containing the N-terminus and VPS9
697 domain are artificially recruited by a YPE endosomal anchor. Insets are scaled to match other regions in
698 the same channel. (G) Quantification of Vps26-mScI puncta per cell. One-way ANOVA with Tukey's
699 multiple comparison test; n = 3, cells/strain/replicate ≥ 750; not significant, n.s. = P > 0.05, *** = P < 0.001,
700 **** = P < 0.0001. Scale bars, 2 µm. Error bars report SEM. OE, overexpressed.

701 **Figure 6. The VINE complex exhibits characteristics of a membrane sorting complex.** (A) Time-lapse
702 imaging of cells co-overexpressing GFP-Vin1 and Vrl1 show tubules emanating from Did2-labeled
703 endosomes. Images were uniformly enlarged using a bicubic expansion function to show detail. Solid
704 arrowheads mark a tubule, open arrowhead marks a scission event. (B) Normalized intensity line scan
705 analysis performed on images from (A) along the yellow dotted line. (C) Punctate localization of GFP-
706 tagged Mrl1, but not other endosomal recycling cargo, is decreased in cells expressing *VRL1*. (D)
707 Quantification of GFP-tagged puncta in WT and *vrl1* strains. Two tailed Welch's t tests; n = 3,
708 cells/strain/replicate ≥ 902; not significant, n.s. = P > 0.05, * = P < 0.05. (E) Mutation of the D373 residue
709 required for VPS9 GEF activity does not prevent Vrl1 from redistributing Mrl1. (F) Quantification of Mrl1-
710 mScI puncta per cell. One-way ANOVA with Tukey's multiple comparison test; n = 3, cells/strain/replicate
711 ≥ 1,788; not significant, n.s. = P > 0.05, * = P < 0.05. (G) Schematic of Vps10 cytosolic tail mutant and
712 Mrl1 cytosolic tail chimera tested for VINE-mediated sorting in (H, I). (H) The Mrl1 cytosolic tail is
713 sufficient to confer VINE-mediated redistribution. (I) Percent of cells showing punctate localization of
714 indicated GFP-tagged constructs. Blind scoring of GFP signal was conducted manually. One-way ANOVA

715 with Tukey's multiple comparison test; n = 3, cells/strain/replicate ≥ 237; not significant, n.s. = P > 0.05,
716 *** = P < 0.001, **** = P < 0.0001. (J) Mrl1-mScI puncta are reduced in a *snx4*Δ strain. (K) Quantification
717 of Mrl1-mScI puncta per cell. One-way ANOVA with Tukey's multiple comparison test; n = 3,
718 cells/strain/replicate ≥ 1,036; not significant, n.s. = P > 0.05, * = P < 0.05, ** = P < 0.01, *** = P < 0.001,
719 **** = P < 0.0001. (L) Model for VINE-mediated sorting of Mrl1. VINE recognizes Mrl1 through its
720 cytosolic tail and transports it from the endosome to the Golgi, where it is subsequently delivered to the
721 vacuolar membrane. Scale bars, 2 µm. Error bars report SEM. OE, overexpressed. TM, transmembrane.
722

723 **Supplemental Figure and Table Legends**

724 **Figure 1 S1. The Vrl1 PX-like domain is missing key PI3P-binding residues.** (A) Results from Phyre2
725 analysis of Vrl1 sequences (Intensive mode, http://www.sbg.bio.ic.ac.uk/phyre2). (B) Sequence alignment
726 of Vrl1 C-terminus (aa 737-1089) with yeast and human PX domain-containing proteins. Canonical PI3P-
727 binding "RRY" motif is absent in Vrl1 (highlighted with red dots above alignment).

728 **Figure 1 S2. The Vrl1 N-terminus and VPS9 domain do not localize.** (A) The Vrl1 N-terminus (aa 1-
729 465) does not localize to puncta when expressed from the endogenous *VRL1* promoter or the strong *ADH1*
730 promoter and instead accumulates in the cytosol. Scale bars, 2 µm.

731 **Figure 2 S1. Vrl1 is indispensable for Vin1 puncta localization.** (A) N-terminally tagged Vin1 requires
732 Vrl1 for localization to puncta at three different expression levels. Insets are scaled to match other regions
733 in the same channel. (B) Overexpression of Vrl1 from the *ADH1* promoter increases the average number
734 of bright Vin1-Envy puncta per cell. (C) Quantification of Vrl1-Envy puncta per cell. One-way ANOVA
735 with Tukey's multiple comparison test; n = 3, cells/strain/replicate ≥ 1,495; *** = P < 0.001, **** = P <
736 0.0001. Scale bars, 2 µm. Error bars report SEM.

737 **Figure 3 S1. Vrl1 does not form a novel retromer-like complex.** (A) Vrl1 does not interact strongly with
738 subunits of retromer by CoIP. (B) Expression of *VRL1* does not rescue loss of endosomal Vps10-Envy in a
739 *vps5*Δ strain. (C) Expression of *VRL1* does not rescue loss of endosomal Vps35-GFP or vacuolar
740 morphology defects in retromer SNX-BAR deletion strains. (D) Quantification of Vps35-GFP puncta per
741 cell. One-way ANOVA with Tukey's multiple comparison test; n = 3, cells/strain/replicate ≥ 1,243; not
742 significant, n.s. = P > 0.05, *** = P < 0.001. Scale bars, 2 µm. Error bars report SEM. OE, overexpressed.

743 **Figure 4 S1. The Vin1 PX-BAR region is indispensable for Vrl1 localization.** (A) The Vin1 N-terminus
744 is not sufficient to localize overexpressed Vrl1-Envy to membranes in a *VIN1* deletion strain. The Vrl1-
745 YPE chimera recruits the Vin1 N-terminal prey construct to puncta in strains lacking the chromosomal copy
746 of *VIN1*. (B) Quantification of RFP puncta per cell. One-way ANOVA with Tukey's multiple comparison

747 test; n = 3, cells/strain/replicate ≥ 1,068; not significant, n.s. = P > 0.05, ** = P < 0.01, *** = P < 0.001,
748 **** = P < 0.0001. Scale bars, 2 µm. Error bars report SEM.

749 **Figure 4 S2. The Vin1 N-terminus has three conserved regions in fungal homologs.** (A) Sequence
750 alignment of Vin1 and Vps5 ohnologs collected using the Yeast Gene Order Browser (http://ygob.ucd.ie/).
751 Three conserved regions were selected for expression as mScI-tagged fragments: $Vin1^{1-29}$ (Region 1),
752 $Vin1^{41-78}$ (Region 2) and $Vin1^{76-95}$ (Region 3).

753 **Figure 6 S1. CRISPR-corrected Vrl1 recruits Vin1 and sorts Mrl1.** (A) Localization of Vin1-mScI in
754 BY4741 (*vrl1*) and an isogenic strain with the *vrl1* mutation corrected at the endogenous *VRL1* locus using
755 CRISPR-Cas9 gene editing technology. Vin1-mScI localizes to puncta in a CRISPR-corrected *VRL1* strain.
756 (B) Mrl1-mScI is redistributed from puncta in the CRISPR-corrected *VRL1* strain. (C) Quantification of
757 large, bright Mrl1-mScI puncta per cell. Two tailed equal variance *t* test; n = 3, cells/strain/replicate ≥ 1,183;
758 ** = P < 0.01. Scale bars, 2 µm. Error bars report SEM.

759 **Table S1. Vrl1 DHFR Interactors.** List of Z-scores from the Vrl1 DHFR screen.

760 **Table S2. Vrl1 DHFR Ontology Enrichment.** List of enriched ontology terms for Vrl1 DHFR interactors
761 (Z > 2).

762 **Table S3. Yeast SNX-BAR Dimer Predictions.** Results of pairwise yeast SNX-BAR prediction matrix
763 performed using ColabFold.

764 **Table S4. List of *Saccharomyces cerevisiae* strains used in this study.**

765 **Table S5. List of plasmids used in this study.**

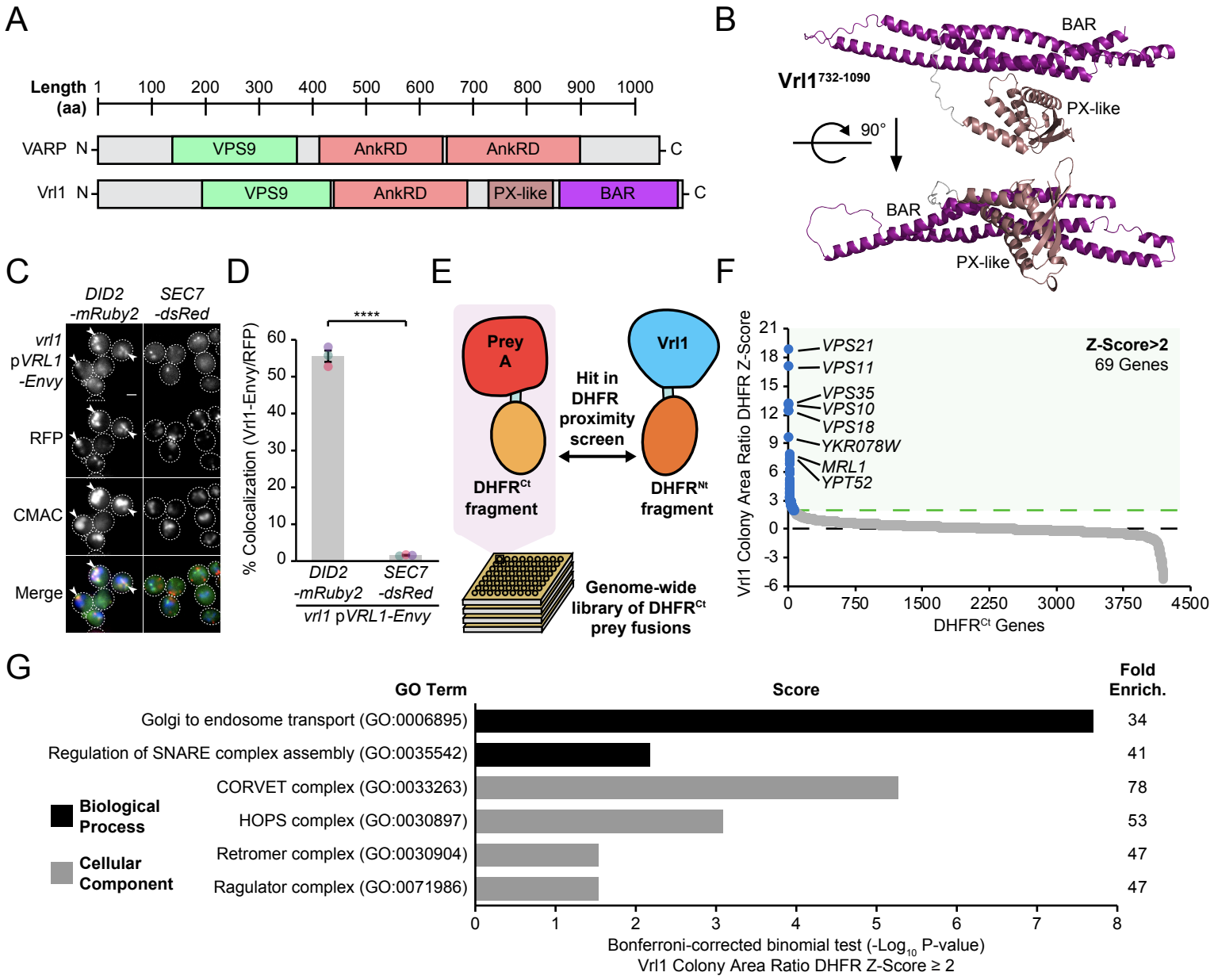

Figure 1, Shortill et al., 2022

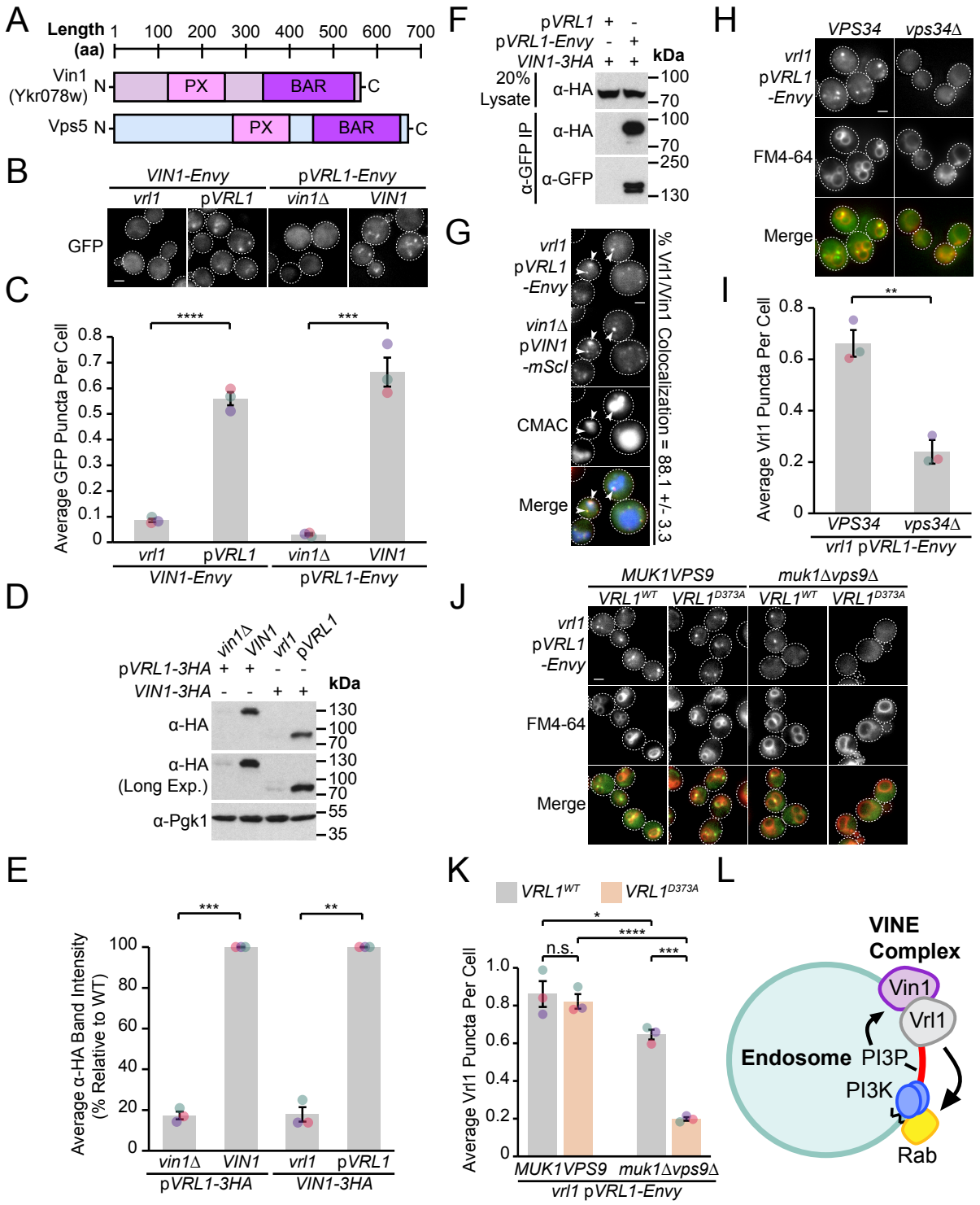

Figure 2, Shortill et al., 2022

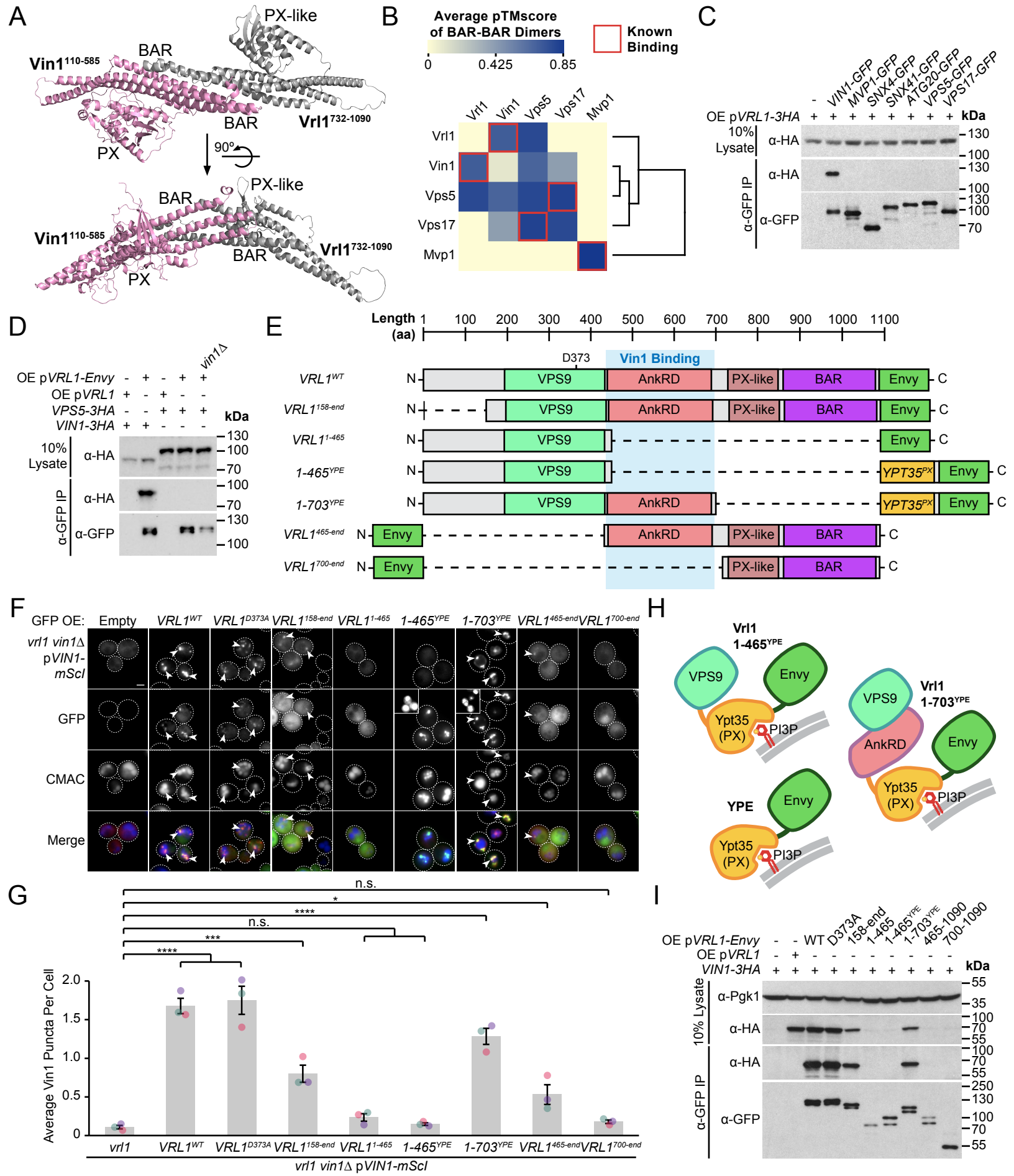

Figure 3, Shortill et al., 2022

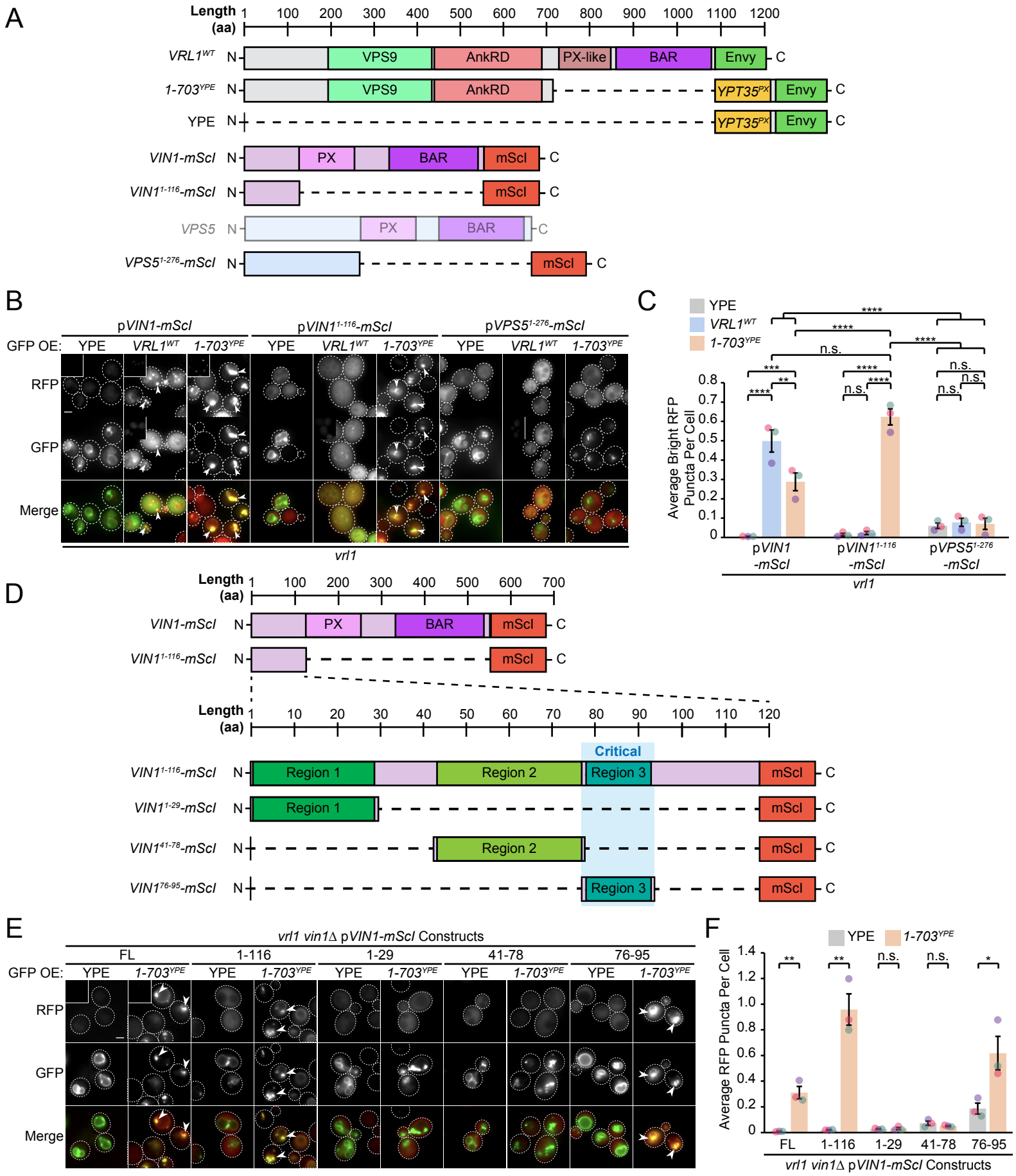

Figure 4, Shortill et al., 2022

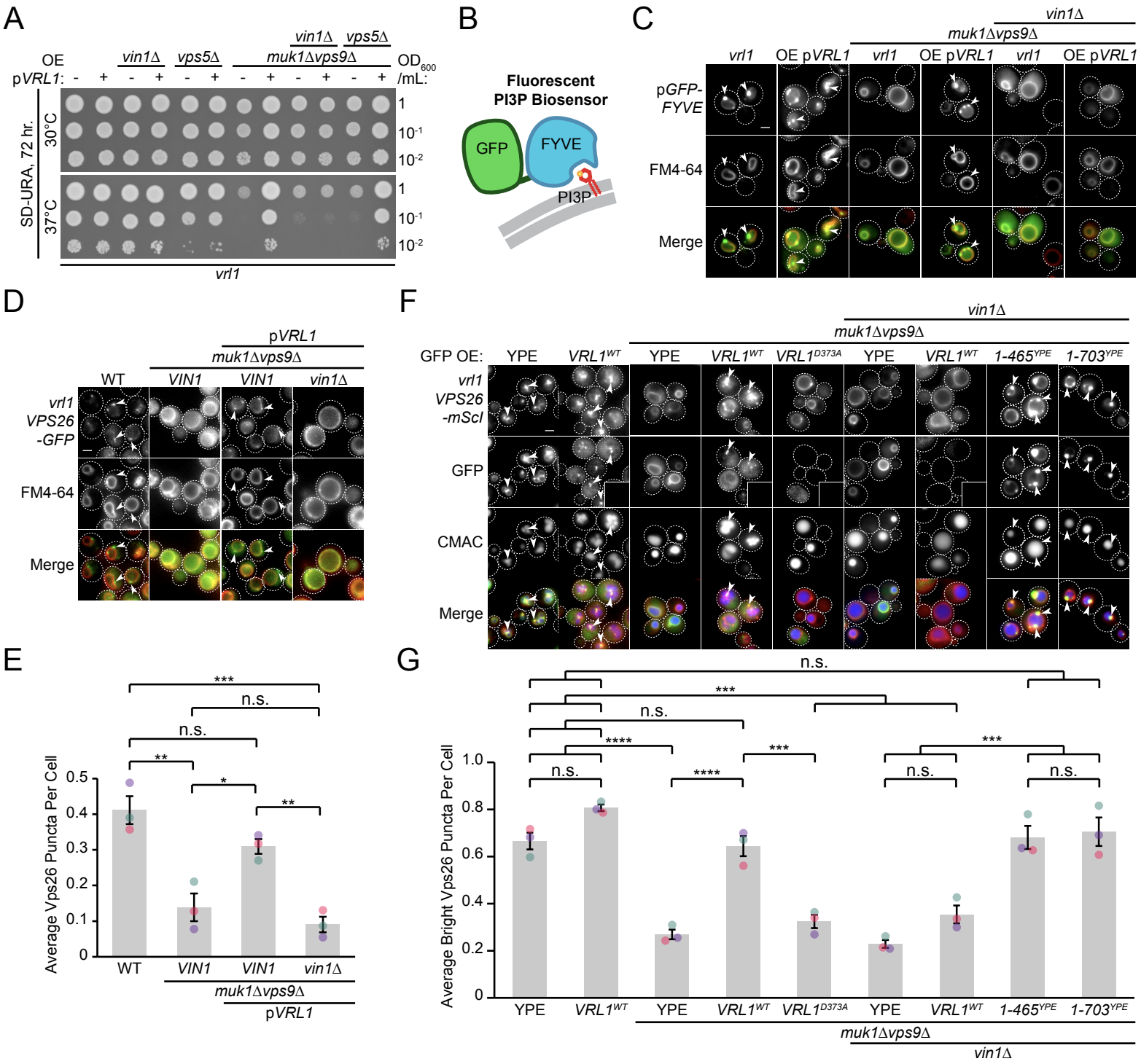

Figure 5, Shortill et al., 2022

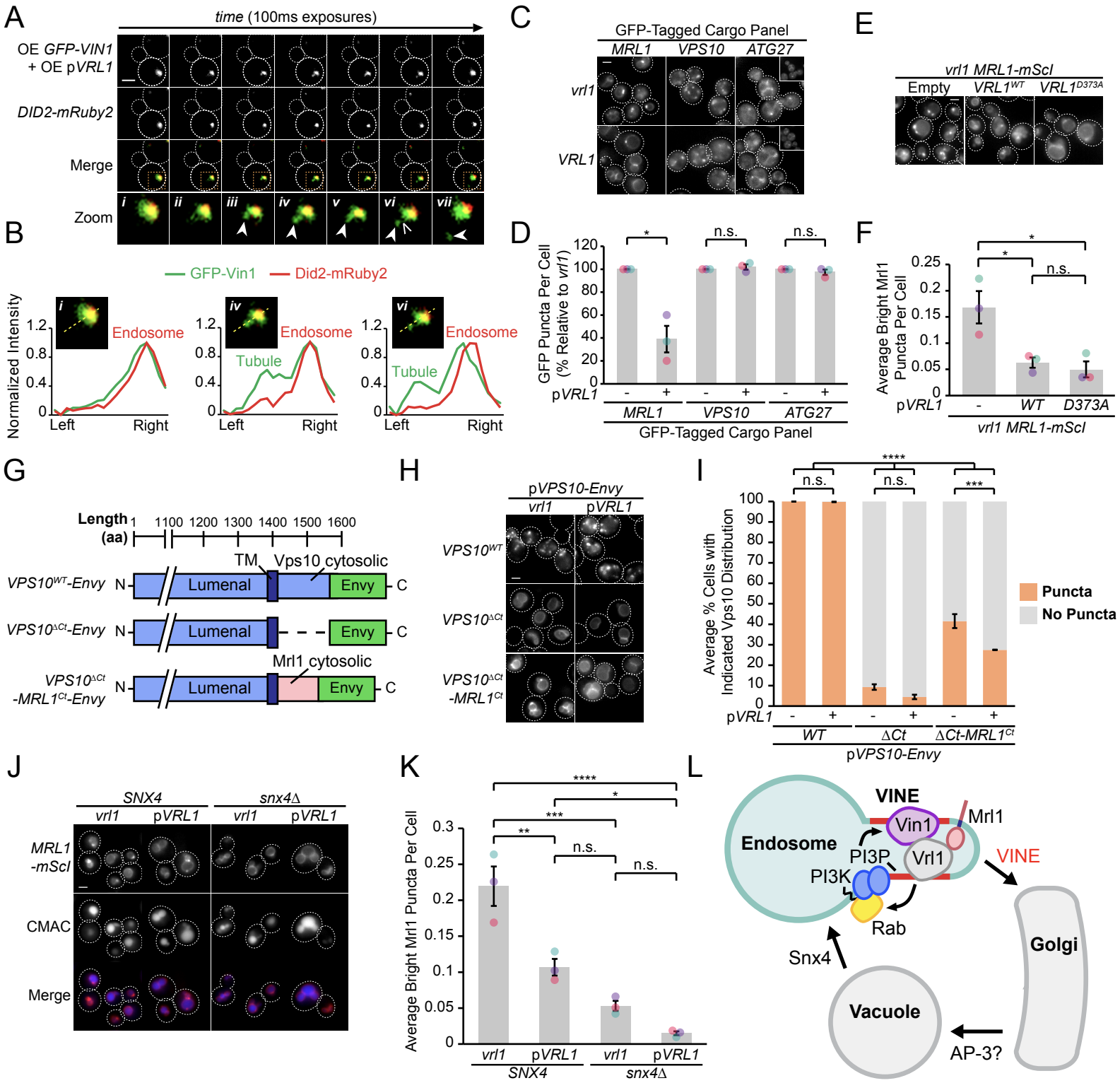

Figure 6, Shortill et al., 2022

A

Domain	Template Identifier	Template Information	Vrl1 Sequence	Identity (%)	Confidence (%)
VPS9	PDB 1txu Chain A	Crystal structure of the VPS9 domain of Rabex-5	189-428	15	99.8
AnkRD	PDB 4rlv Chain A	Crystal structure of the AnkB 24 Ankyrin repeats in complex with AnkR autoinhibition segment	444-689	17	100
PX-like/BAR	PDB 6q0x Chain D	The cryo-EM structure of the SNX-BAR Mvp1 tetramer	737-1089	11	98.6

B

Figure 1 S1, Shortill et al., 2022

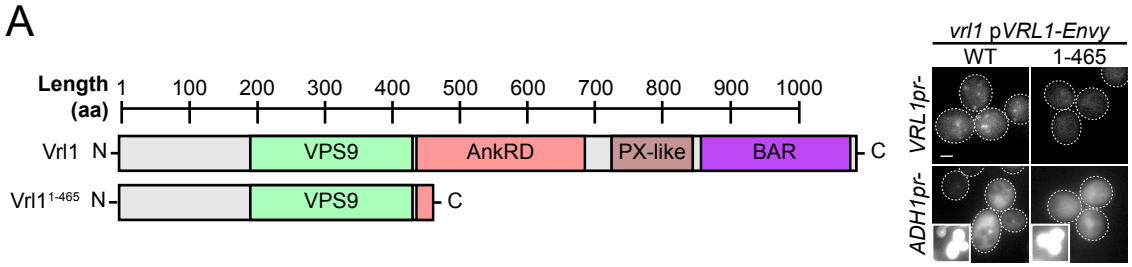

Figure 1 S2, Shortill et al., 2022

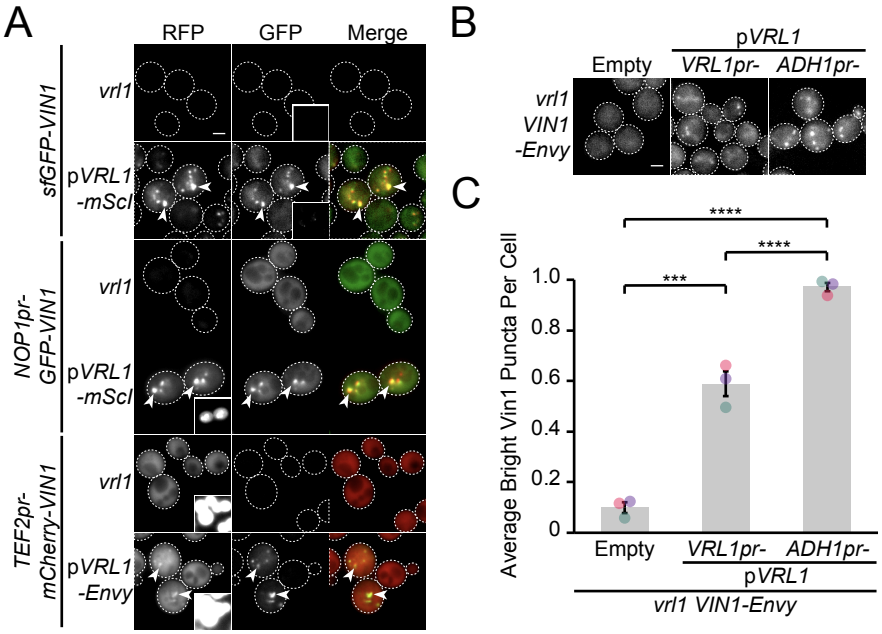

Figure 2 S1, Shortill et al., 2022

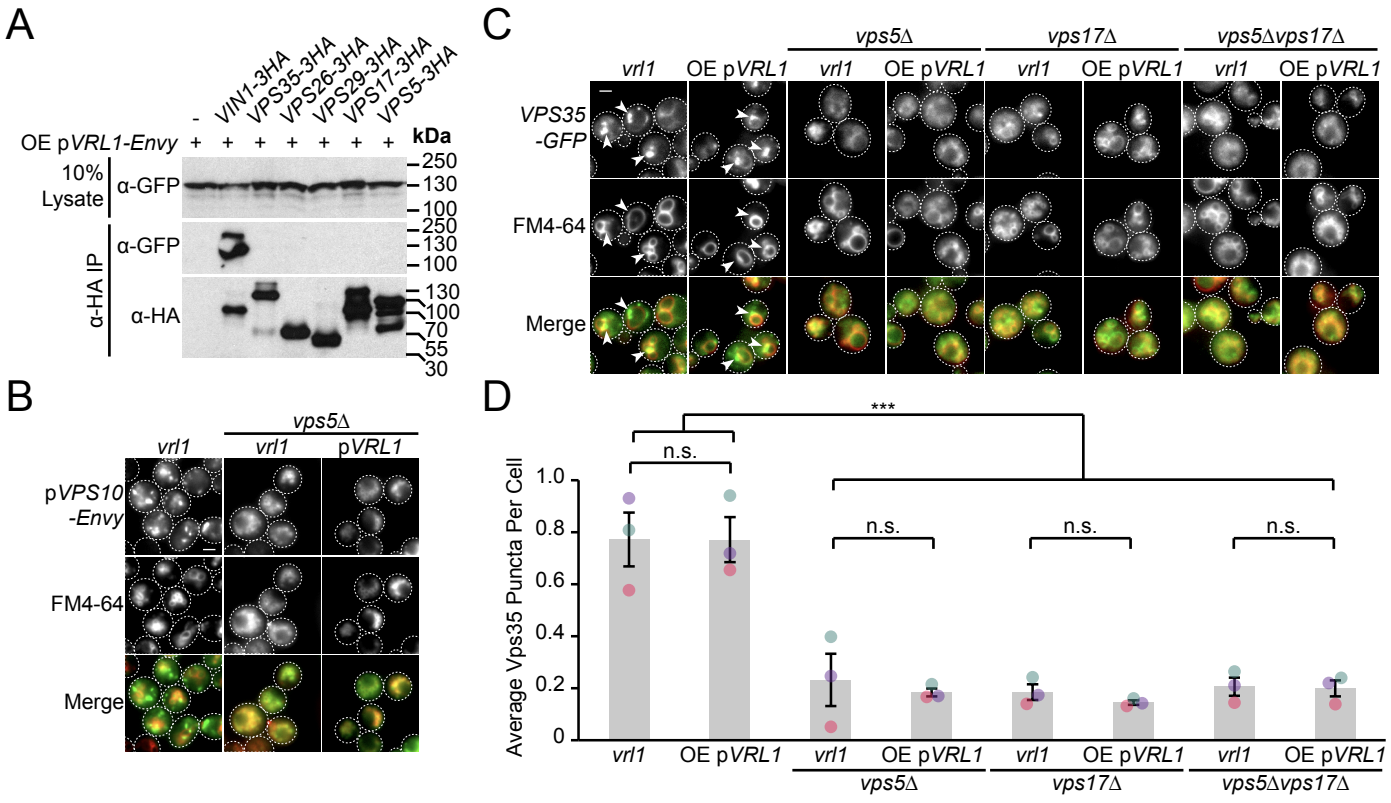

Figure 3 S1, Shortill et al., 2022

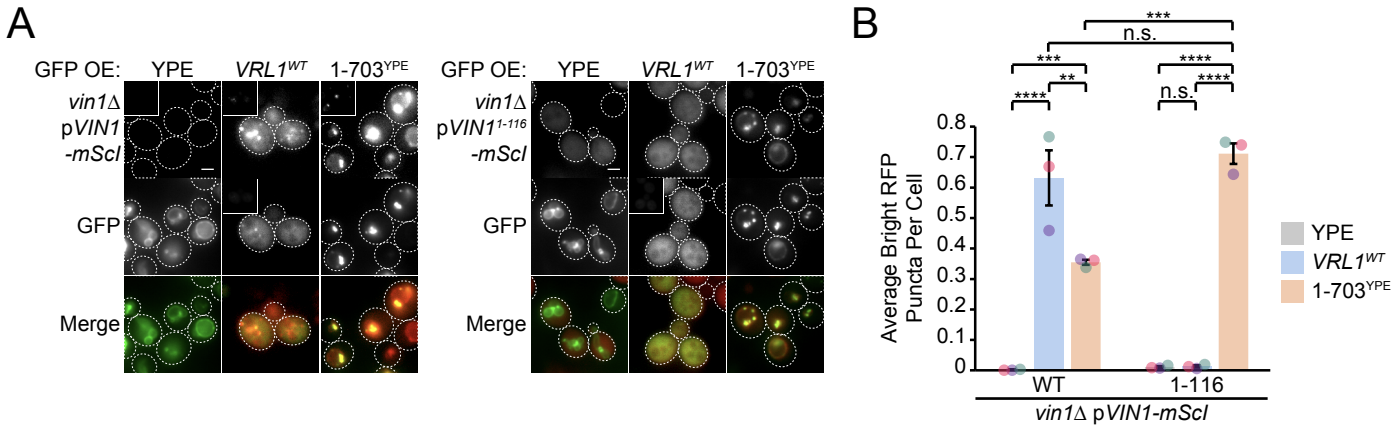

Figure 4 S1, Shortill et al., 2022

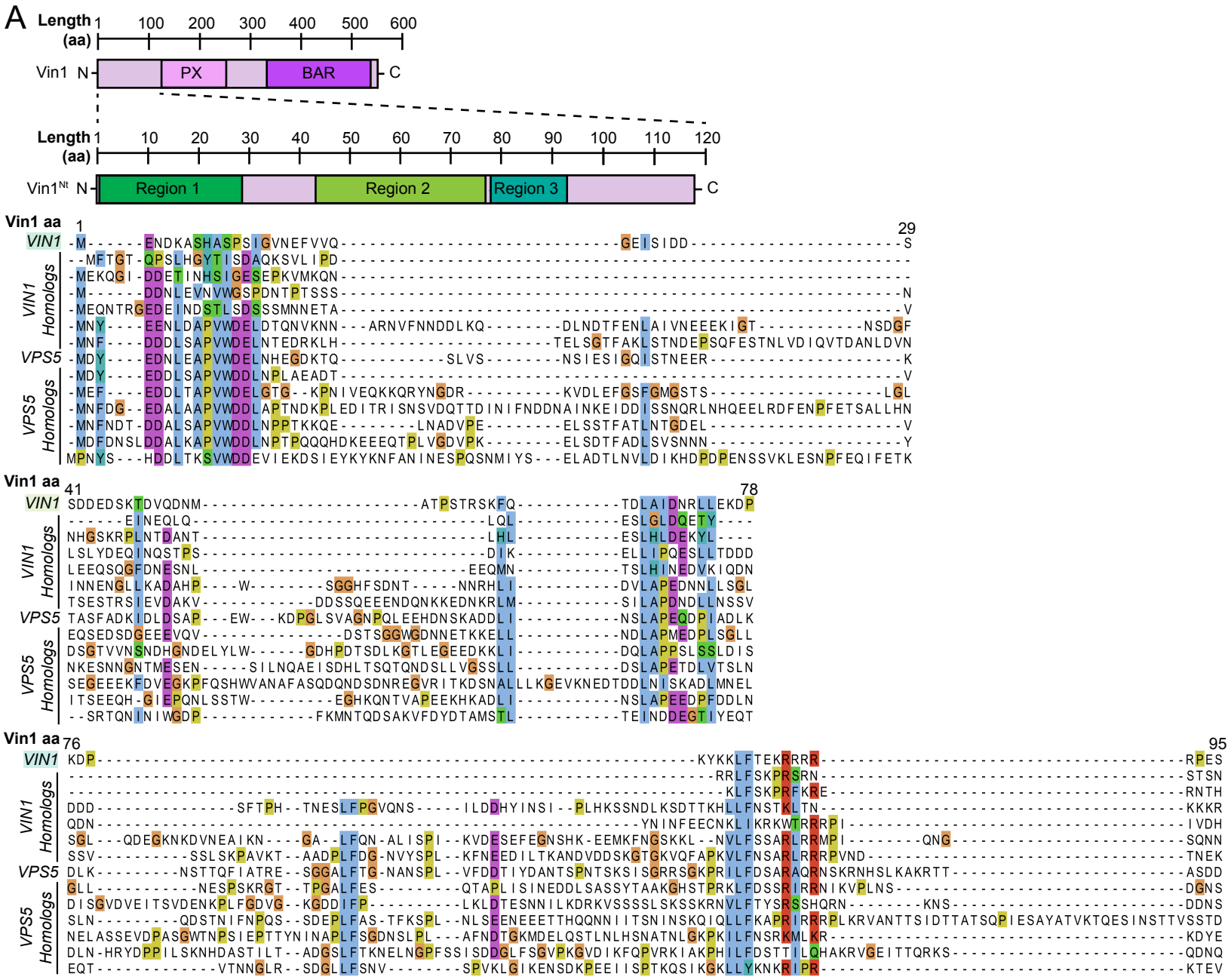

Figure 4 S2, Shortill et al., 2022

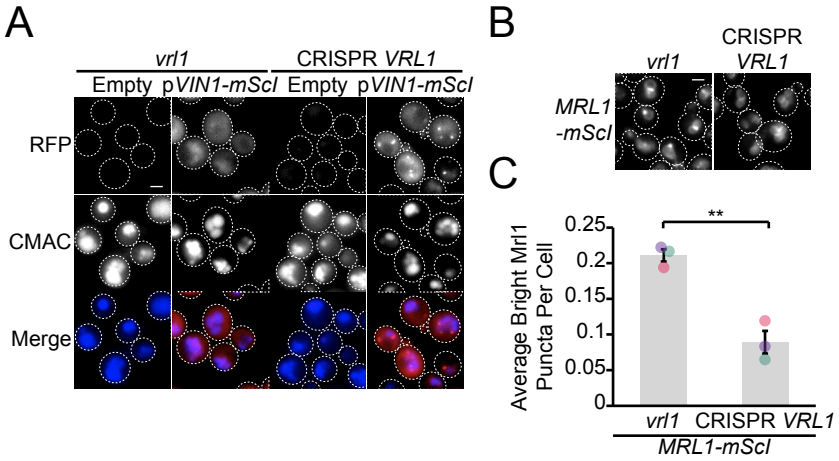

Figure 6 S1, Shortill et al., 2022